

FILE COP
AD-A201 676

(2)

NAVAL POSTGRADUATE SCHOOL

Monterey, California



THESIS

Natural Convection Liquid Immersion Cooling
of a Column of Discrete Heat Sources
in a Vertical Channel

by

Daniel L. Knight
September 1988

Thesis Advisor:

Yogendra Joshi

Approved for public release; distribution is unlimited

DTIC
ELECTE
DEC 27 1988
S E D

88 12 27 169

UNCLASSIFIED

SECURITY CLASSIFICATION OF THIS PAGE

REPRODUCED AT GOVERNMENT EXPENSE

REPORT DOCUMENTATION PAGE

1a. REPORT SECURITY CLASSIFICATION UNCLASSIFIED		1b. RESTRICTIVE MARKINGS	
2a. SECURITY CLASSIFICATION AUTHORITY		3. DISTRIBUTION/AVAILABILITY OF REPORT Approved for public release; distribution is unlimited	
2b. DECLASSIFICATION/DOWNGRADING SCHEDULE			
4. PERFORMING ORGANIZATION REPORT NUMBER(S)		5. MONITORING ORGANIZATION REPORT NUMBER(S)	
6a. NAME OF PERFORMING ORGANIZATION Naval Postgraduate School	6b. OFFICE SYMBOL (If applicable) 69	7a. NAME OF MONITORING ORGANIZATION	
6c. ADDRESS (City, State, and ZIP Code) Monterey, California 93943-5000		7b. ADDRESS (City, State, and ZIP Code) Monterey, California 93943-5000	
8a. NAME OF FUNDING/SPONSORING ORGANIZATION	8b. OFFICE SYMBOL (If applicable)	9. PROCUREMENT INSTRUMENT IDENTIFICATION NUMBER	
8c. ADDRESS (City, State, and ZIP Code)		10. SOURCE OF FUNDING NUMBERS	
		PROGRAM ELEMENT NO.	PROJECT NO.
		TASK NO.	WORK UNIT ACCESSION NO.
11. TITLE (Include Security Classification) Natural Convection Liquid Immersion Cooling of a Column of Discrete Heat Sources in a Vertical Channel			
12. PERSONAL AUTHOR(S) KNIGHT, Daniel L.			
13a. TYPE OF REPORT Master's Thesis	13b. TIME COVERED FROM _____ TO _____	14. DATE OF REPORT (Year, Month, Day) 1988 September	15. PAGE COUNT 63
16. SUPPLEMENTARY NOTATION The views expressed in this thesis are those of the author and do not reflect the official policy or position of the Department of Defense or the US Government			
17. COSATI CODES		18. SUBJECT TERMS (Continue on reverse if necessary and identify by block number) Convective Flow, Thermal Transport, Flow Visualization, Theses. (Jd)	
FIELD	GROUP	19. ABSTRACT (Continue on reverse if necessary and identify by block number) Natural convection from a single column of eight in-line, rectangular, flush heat sources was examined. A vertical channel was formed by placing a movable shroud parallel to the test surface. The experimental program consisted of temperature measurements and flow visualizations. For a range of component power levels and channel spacings, surface temperatures of each heat source were measured at five locations using embedded thermocouples. The resulting steady state data was compared with corresponding measurements for an identical geometric arrangement of protruding heat sources. The flow visualization was carried out using a laser generated plane of light. <i>Keywords:</i>	20. DISTRIBUTION/AVAILABILITY OF ABSTRACT <input checked="" type="checkbox"/> UNCLASSIFIED/UNLIMITED <input type="checkbox"/> SAME AS RPT. <input type="checkbox"/> DTIC USERS
22a. NAME OF RESPONSIBLE INDIVIDUAL Prof Joshi		21. ABSTRACT SECURITY CLASSIFICATION UNCLASSIFIED	22b. TELEPHONE (Include Area Code) (408)646-3400
		22c. OFFICE SYMBOL 69Ji	

DD FORM 1473, 84 MAR

83 APR edition may be used until exhausted.

All other editions are obsolete

SECURITY CLASSIFICATION OF THIS PAGE

* U.S. Government Printing Office: 1980-000-04.

UNCLASSIFIED

Approved for public release; distribution is unlimited

Natural Convection Liquid Immersion Cooling of a Column of Discrete Heat Sources in a Vertical Channel

by

Daniel L. Knight
Lieutenant, United States Navy
B.S., The Citadel, 1979

Submitted in partial fulfillment of the
requirements for the degree of

MASTER OF SCIENCE
IN MECHANICAL ENGINEERING

from the

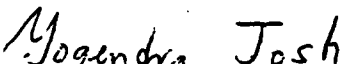
NAVAL POSTGRADUATE SCHOOL

September 1988

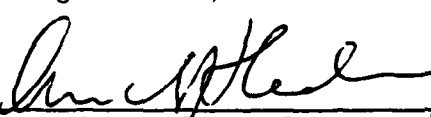
Author:


Daniel L. Knight

Approved by:


Yogendra Joshi

Yogendra Joshi, Thesis Advisor


Anthony J. Healey

Chairman
Department of Mechanical Engineering


Gordon E. Schacher

Dean of Science and Engineering

ABSTRACT

Natural convection from a single column of eight in-line, rectangular, flush heat sources was examined. A vertical channel was formed by placing a movable shroud parallel to the test surface. The experimental program consisted of temperature measurements and flow visualizations. For a range of component power levels and channel spacings, surface temperatures of each heat source were measured at five locations using embedded thermocouples. The resulting steady state data was compared with corresponding measurements for an identical geometric arrangement of protruding heat sources. The flow visualization was carried out using a laser generated plane of light.

<u>Accession For</u>	
NTIS GRA&I <input checked="" type="checkbox"/>	
DTIC TAB <input type="checkbox"/>	
Unannounced <input type="checkbox"/>	
<u>Justification</u>	
By _____	
<u>Distribution/</u>	
<u>Availability Codes</u>	
Dist	Avail and/or
	Special
A-1	



TABLE OF CONTENTS

I.	INTRODUCTION	1
	A. STATEMENT OF PROBLEM	1
	B. OBJECTIVES	2
II.	EXPERIMENTAL	4
	A. GENERAL DESIGN CONSIDERATION	4
	B. EXPERIMENTAL PROCEDURE	7
	C. DATA ANALYSIS	8
III.	TRANSPORT ADJACENT TO AN ISOLATED VERTICAL SURFACE	12
	A. FLOW VISUALIZATION	12
	B. QUANTITATIVE	15
	C. EFFECT OF COMPONENT SPACING ON HEAT TRANSFER .	17
	D. TEMPERATURE MEASUREMENTS WITHIN THE FLUID . .	22
IV.	TRANSPORT IN A VERTICAL CHANNEL	28
	A. FLOW VISUALIZATION	28
	B. QUANTITATIVE	28
V.	CONCLUSIONS	39
VI.	RECOMMENDATIONS	40
APPENDIX A	41
	A. TEMPERATURE ACQUISITION PROGRAM	41
	B. DATA REDUCTION PROGRAM	44
APPENDIX B	47
	A. SAMPLE CALCULATIONS	47
	1. CHARACTERISTIC DIMENSIONS	47

2. CONDUCTION LOSS	47
3. CONVECTED HEAT FLUX	47
4. FLUID PROPERTIES	48
5. NON-DIMENSIONAL TEMPERATURE EXCESS	48
6. HEAT TRANSFER COEFFICIENT	49
7. FLUX-BASED GRASHOF NUMBER	49
8. NUSSELT NUMBER	49
LIST OF REFERENCES	50
INITIAL DISTRIBUTION LIST	51

LIST OF FIGURES

2.1 Assembled Test Surface	5
2.2 Foil Heater	6
2.3 Traversing Thermocouple Probe	7
2.4 Laser and Camera Arrangement for Photography in the x-y Plane. . .	9
3.1 Steady Flow in the x-y Plane for Power Levels of 0.2, 1.0 and 2.0 Watts	13
3.2 Flow in the x-z Plane at 0.2, 1.0 and 2.0 Watts	14
3.3 Non-dimensional Temperature Excess vs. Position: 2.0 Watts	16
3.4 Data for Nusselt Number vs. Flux-Based Grashof Number	18
3.5 Modified Nusselt Number vs. Flux-Based Grashof Number with Least Squares Fit	19
3.6 Non-dimensional Temperature Excess vs. Position with Four Elements Powered	20
3.7 Non-dimensional Temperature Excess vs. Position with Three Elements Powered	21
3.8 Nusselt Number vs. Flux-based Grashof Number with Four Elements Powered	23
3.9 Nusselt Number vs. Flux-based Grashof Number with Three Elements Powered	24
3.10 Fluid Temperature Distribution in the y-Direction for 0.2 and 1.0 Watts	26
3.11 Spanwise Fluid Temperature Distribution	27
4.1 Steady Flow in the x-y Plane for Power Levels of 0.2, 1.0 and 2.0 Watts with 12 mm Shroud	29

4.2 Steady Flow in the x-y Plane for Power Levels of 0.2, 1.0, 2.0 Watts with 15 mm Shroud	30
4.3 Flow in the x-z Plane with 6 mm Shroud Wall	31
4.4 Non-dimensional Temperature Excess vs. Position with Shroud at 0.2 Watts	33
4.5 Non-dimensional Temperature Excess vs. Position with Shroud at 2.0 Watts	34
4.6 Temperature Difference vs. Shroud Spacing: 2.0 Watts	35
4.7 Modified Nusselt Number vs. Flux-based Grashof Number with Shroud at 1.5 mm	36
4.8 Modified Nusselt Number vs. Flux-based Grashof Number with Shroud at 6.0 mm	38

LIST OF SYMBOLS

<u>Symbol</u>	<u>Description</u>	<u>Units</u>
A	Area	m^2
A_s	Heater Surface Area	m^2
g	Acceleration due to Gravity	$\frac{m}{s^2}$
Gr^*	Flux-based Grashof Number	Dimensionless
h	Heat Transfer Coefficient	$\frac{W}{m^2 K}$
k_f	Fluid Thermal Conductivity	$\frac{W}{m K}$
k_{pg}	Plexiglass Thermal Conductivity	$\frac{W}{m K}$
L	Test Surface Length	m
\bar{L}	Characteristic Length	m
Nu	Nusselt Number	Dimensionless
Nu^*	Modified Nusselt Number	Dimensionless
NDT	Non-dimensional Temperature Excess	Dimensionless
P	Prandtl Number	Dimensionless
q''	Energy Flux Convected into the Fluid per Component	$\frac{W}{m^2}$
Q_{COND}	Energy Loss via Conduction Through the Test Surface	W
Q_{CONV}	Energy Convected into the Fluid per Component	W
Q_{in}	Energy into each Heater	W
S_n	Heater Element Number in Relation to the Leading Component	Dimensionless

T	Local Surface Temperature	°C
T_{amb}	Ambient Temperature	°C
T_{avg}	Average Component Temperature	°C
T_{film}	Film Temperature at which Fluid Properties are Evaluated	K
T_s	Surface Temperature	°C
v	Specific Volume	$\frac{m^3}{kg}$
x	Vertical Distance from Bottom	m
	Edge of Test Surface	
z	Horizontal Distance from Component Center	m
β	Expansion Coefficient	$\frac{1}{K}$
μ	Dynamic Viscosity	$\frac{N \cdot s}{m^2}$
ν	Kinematic Viscosity	$\frac{m^2}{s}$
θ	Temperature Difference Between Local Temperature and Ambient	K
θ_o	Temperature Scaling Factor	K

ACKNOWLEDGMENT

Natural convection from a single column of eight in-line, rectangular, flush heat sources was examined. A vertical channel was formed by placing a movable shroud parallel to the test surface. The experimental program consisted of temperature measurements and flow visualizations. For a range of component power levels and channel spacings, surface temperatures of each heat source were measured at five locations using embedded thermocouples. The resulting steady state data was compared with corresponding measurements for an identical geometric arrangement of protruding heat sources. The flow visualization was carried out using a laser generated plane of light.

I. INTRODUCTION

A. STATEMENT OF PROBLEM

With each successive increase in the scale of integration of micro-electronic circuits, there has been a need to improve cooling technologies. Currently, chip heat fluxes are approaching 50 W/cm^2 , [Ref. 1]. Heat dissipation may be improved by using higher velocities of air, chilled water heat exchangers, or altering the system design to reduce its thermal resistance. These techniques are becoming less satisfactory and the limits of air and indirect liquid cooling have nearly been reached. If projected heat fluxes of 200 W/cm^2 , [Ref. 1], are to be achieved, then direct liquid immersion becomes an attractive option, [Ref. 1, 6].

The performance and reliability of micro-electronic devices are very sensitive to junction temperatures. The failure rate of chips increase exponentially as the junction temperature increases. The long term reliability of circuit chips can be improved by 50% with every 10°C decrease in temperature that the device is maintained below its maximum operating temperature, [Ref. 2, 3, 4].

For a complete thermal analysis of any electronic package design, all three modes of heat transfer must be considered. Radiation effects are significant primarily in systems involving air cooling. Effects of conduction, however, must be evaluated in each cooling application. These may also be substantial during transients.

The convection heat transfer rate from a surface at temperature T_s with exposed surface area A to its surrounding fluid at temperature T_{amb} is given by Newton's Law of Cooling:

$$q = hA(T_s - T_{amb}) \quad (1.1)$$

This is the definition of h , the convective heat transfer coefficient and not a phenomenological law.

Most available correlations for the convective heat transfer coefficient are usually valid for large heat sources. These are often good for determining the overall heat transfer from a single circuit board. Individual devices mounted on the substrate act as discrete heat sources and typically have higher average temperatures than those predicted by such text book correlations [Ref. 6].

Convection may be either forced or natural. Forced convection relies on a prime mover to displace the fluid and cause it to flow over the electronic package. This method of convection yields very high heat transfer coefficients and may become one of the primary means of cooling electronic packages as component heat fluxes continue to rise. Natural convection or buoyancy induced flow, results from body forces acting on density differences within the fluid. In many applications, these density gradients result due to the presence of temperature variations. The heat transfer coefficients are smaller than those associated with forced convection since the flow velocities are generally much smaller for natural convection. However, the resulting design of the package can be considerably simpler and more reliable than in other cooling arrangements.

B. OBJECTIVES

This experimental study was undertaken to determine the hydrodynamic and thermal characteristics of buoyancy induced flow resulting from several flush mounted

discrete heat sources on a vertical surface. The results from this study will be compared to those in Reference 7 where an array of rectangular protruding heat sources was used.

A single column of discrete heat sources was chosen since it provided a simple geometric arrangement simulating some of the modern electronic packages such as flat packs.

Specific objectives of this study were:

- To visualize the steady-state natural convection flow within a channel over a range of component power levels and channel widths.
- To measure component temperatures at each power level and channel width and develop heat transfer relationships for this geometry.
- To measure the temperature distribution within the fluid adjacent to the heated surface in the absence of a shrouding wall.

This study advances the work described in References 5 and 7 and is part of an ongoing effort to study natural convection liquid immersion cooling of electronic equipment.

II. EXPERIMENTAL

A. GENERAL DESIGN CONSIDERATION

Equipment design and construction details are provided in Reference 5. Only system changes and a brief overview is presented here.

As seen in Figure 2.1, the test assembly consists of eight flush mounted foil heaters. Each heater (Figure 2.2) is a network of Inconel 600 conductor mounted on a Kapton backing. The heaters measured 23.9 mm in width by 7.8 mm in height. They formed a single column on a plexiglass substrate. The substrate measured 25.4 mm square and was 12.7 mm thick. The column of heaters was centered on the substrate and each heater was spaced 25.4 mm center to center from an adjacent heater. Another piece of plexiglass identical to the substrate without the heaters was used as an adjustable shroud wall to form the channel. This shroud was used to simulate the back side of a neighboring circuit board.

Five copper-constantan thermocouples of 0.127 mm diameter wire were used for temperature measurements on each heater. The thermocouples were embedded within 6 mm deep slots in the substrate. For each heater, one thermocouple bead was located at the foil center and the remaining four were at the centers of each edge of the heater. All wires were routed along 6 mm deep grooves cut below the heater placement slots. All wiring came out through the back of the test surface through drilled holes in the substrate. After all heaters and wires were in place, these holes were sealed with a low conductivity adhesive. Omega Bond 101, a high conductivity adhesive, was used to bond the thermocouples in place and to electrically insulate the thermocouple beads from the heater foils. A sixth thermocouple for each heater



Figure 2.1: Assembled Test Surface

was centered behind the heater on the back side of the plexiglass substrate. This was used to estimate conduction losses through the substrate.

A 0.127 mm diameter, copper-constantan thermocouple probe (Figure 2.3) was constructed. This probe was attached to a three dimensional traverse and used to measure the temperature distribution within the fluid adjacent to the test surface. The foil heaters were powered using a regulated D.C. power supply as described in Reference 5.

The test surface was immersed in an open, one cubic meter tank constructed from plate glass and insulated on all sides. For flow visualization, particles of pliolite were suspended in the de-ionized water. Pliolite is an inert substance with a specific gravity of 0.93. These particles were illuminated by aiming an eight milliwatt helium neon laser through a cylindrical lens to split the light beam into a plane of light.

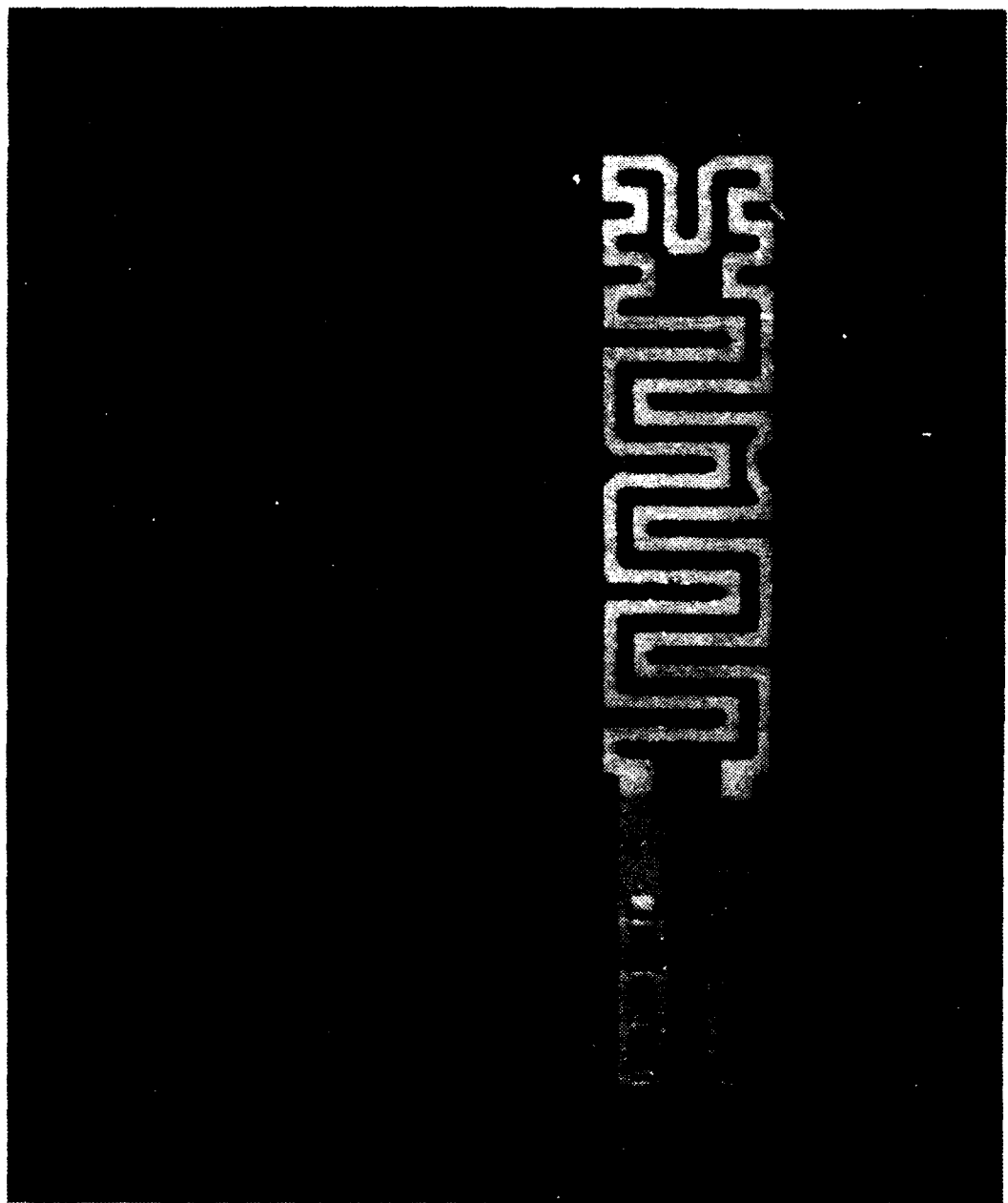


Figure 2.2: Foil Heater

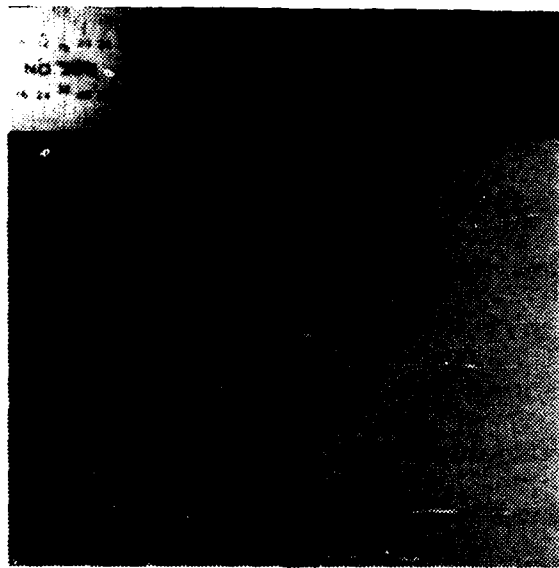


Figure 2.3: Traversing Thermocouple Probe

By using a motor driven camera and an intervalometer, extended time exposure photographs of the flow patterns within the illuminated plane were obtained.

B. EXPERIMENTAL PROCEDURE

Details of data acquisition techniques are provided in Reference 5, hereafter referred to as the initial study. The follow-on study by Willson [Reference 7] will be referred to as the previous study.

Power settings of 0.2, 0.5, 1.0, 1.2, 1.5, and 2.0 watts were used for each channel width. The shroud was adjusted for channel spacings of 1.5 mm, 3.0 mm, 5.0 mm, 9.0 mm, 12.0 mm and 15.0 mm. With the shroud removed, an infinite channel spacing was created.

When measuring the steady state temperatures of each heater element, measurements were taken at 10 minute intervals and compared with the previous data

run. When all thermocouple measurements varied less than 0.05°C , the final steady state temperature measurements were recorded. The temperature acquisition program of the previous study [Appendix A] was executed to record and store data.

Ambient temperature was the average temperature from three thermocouples located in the fluid near the top, bottom and center of the tank. All experiments were stopped if these three temperatures varied by more than 0.1°C .

When measuring the fluid temperature with the movable probe, the data acquisition computer was programmed to continuously monitor the voltage output from the traversing thermocouple probe. This allowed for point to point temperature measurements within the flow.

After all data was recorded, the substrate was painted black to minimize light reflection. Particles of pliolite were mixed with the distilled water to visualize fluid flow. The *f* stop of the camera was set to 2.8 and exposure time for all photographs was 20 seconds. The camera was mounted on a tripod, approximately three inches from the glassplate wall of the tank. Camera height was adjusted and the laser was aligned so that all eight heater surfaces would be in the field of view. When the shroud was in position, the camera angle was inclined slightly to avoid the undesirable light reflection off the shroud. A shroud spacing of 12 mm from the substrate was the minimum channel width at which useful pictures could be taken. Figure 2.4 shows the arrangement of the camera, laser and test surface.

C. DATA ANALYSIS

The convected rate of energy from each heater was determined using an energy balance where:

$$Q_{CONV} = Q_{in} - Q_{COND} \quad (2.1)$$

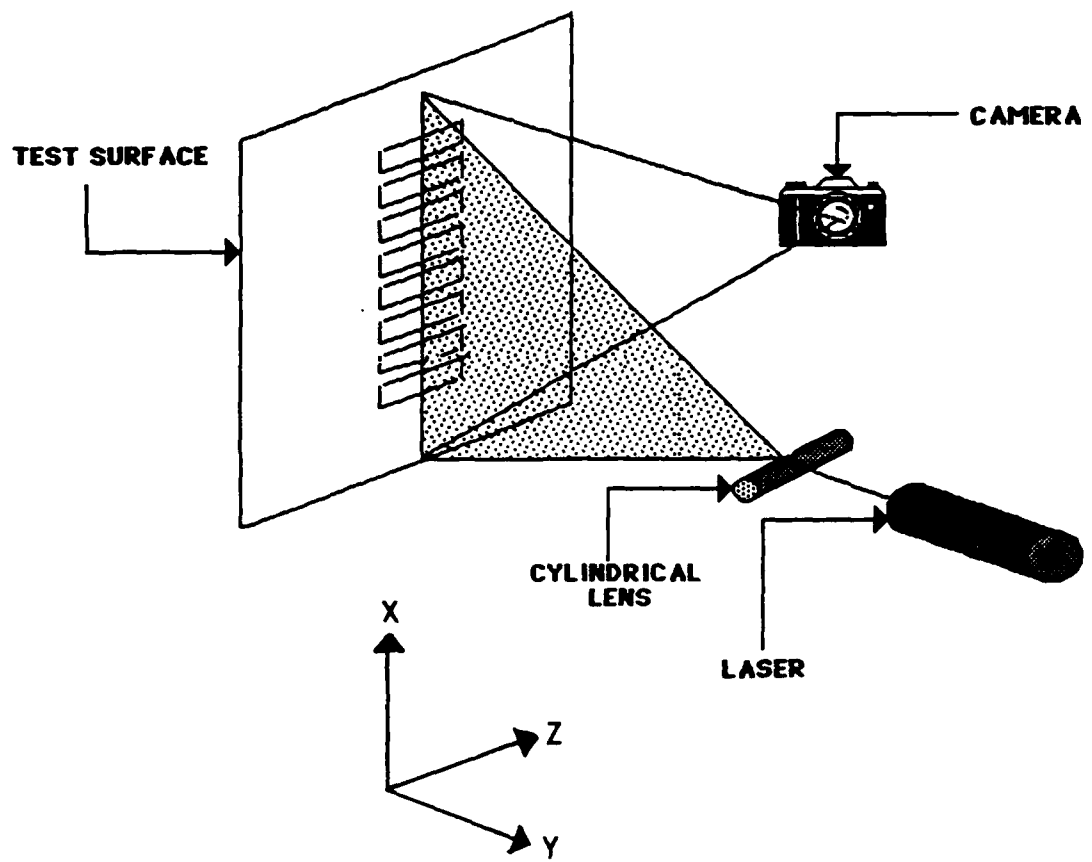


Figure 2.4: Laser and Camera Arrangement for Photography in the x-y Plane.

The energy in Q_{in} was regulated by the power supply and determined as described in the initial study. The energy loss by conduction was estimated by using Fourier's law of conduction for one dimension:

$$Q_{COND} = A_s k_{pg} \frac{\Delta T_{avg}}{\Delta x} \quad (2.2)$$

A_s is the surface area of each heater element, k_{pg} is the thermal conductivity for plexiglass. ΔT_{avg} is the temperature difference between the temperature average of the five thermocouple locations on the heater and the temperature at the back side of the substrate. Δx represents the minimum thickness of the substrate accounting for the grooves cut for wire routing.

A characteristic length, \bar{L} , based on the geometric dimensions of the heaters was chosen for determining non-dimensional temperature excess, θ_o , a flux based Grashof number, Gr^* , and Nusselt number, Nu.

The characteristic length is the heater surface area divided by the heater perimeter.

$$\bar{L} = \frac{A_s}{p} \quad (2.3)$$

Local heat transfer relationships were determined by the following equations:

$$q'' = \frac{Q_{CONV}}{A_s} \quad (2.4)$$

$$\theta_o = \frac{q'' \bar{L}}{k_f} \quad (2.5)$$

$$h = \frac{q''}{\Delta T} \quad (2.6)$$

$$Gr^* = \frac{g\beta q'' \bar{L}^4}{k_f \nu^2} \quad (2.7)$$

$$Nu = \frac{h \bar{L}}{k_f} \quad (2.8)$$

$$\theta = \Delta T \quad (2.9)$$

$$NDT = \frac{\theta}{\theta_o} \quad (2.10)$$

The data reduction program [Appendix A] was used for all calculations. Sample calculations are contained in Appendix B. The various symbols used above are defined in the List of Symbols.

Fluid properties were determined from curve fits listed by Willson [Reference 7]. These are based on the data provided in Incropera and Dewitt [Reference 8]. All properties were evaluated at a film temperature. The film temperature was determined for each case from the local and ambient temperatures.

A non-dimensional length, $\frac{X}{L}$, was used in the presentation of the data. The vertical length $\frac{X}{L}$ is the distance from the bottom edge of the substrate to the local point of interest divided by the overall length of the substrate.

Quantitive developments were expressed as plots of:

- Nu vs. Gr^*
- Non-dimensional local temperature excess vs. local thermocouple location.
- Temperature distribution in the fluid adjacent to the test surface.

III. TRANSPORT ADJACENT TO AN ISOLATED VERTICAL SURFACE

A. FLOW VISUALIZATION

Photographs of the steady state natural convection flow in the x-y plane are shown in Figure 3.1. The laser was aligned so that the plane of light would pass through the geometric center of the heated region of each component. This figure presents all elements at input power levels of 0.2, 1.0 and 2.0 watts respectively from left to right.

Buoyancy forces near the heaters create a strong upward flow. The flow appears to be laminar and is parallel to the substrate after the first component. A boundary layer begins to develop out from the leading heater. The boundary layer thickness increases to about 2.5 component heights at the trailing element. At 1.0 watt, the boundary layer is about 2.0 component heights thick and decreases to about 1.0 component height in thickness at the trailing element for 2.0 watts. The fluid velocity increases and the thickness of the boundary layer decreases with increasing component power input. Ambient fluid is entrained below and along the length of the boundary layer. Figure 3.2 visualizes the flow in the x-z plane at the respective power levels of the previous figure. The flow is vertical along the array for about the width of the heated region of the strips. Weak entrainment from the sides is evident. Side entrainment increases with increasing component heat input. Figure 3.2 clearly shows that for the region along the array, the flow can be treated to an excellent approximation as two dimensional.

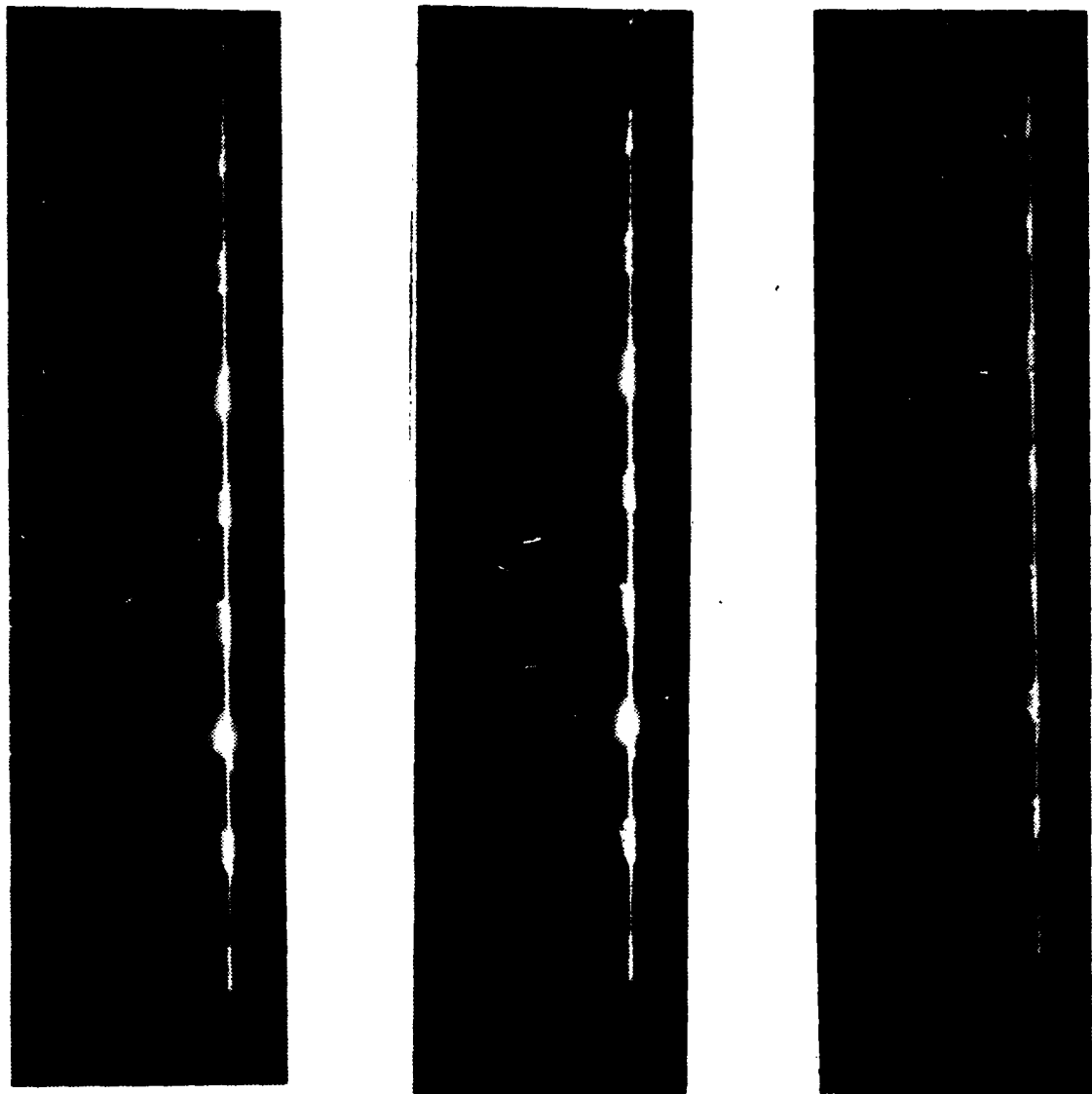


Figure 3.1: Steady Flow in the x-y Plane for Power Levels of 0.2, 1.0 and 2.0 Watts

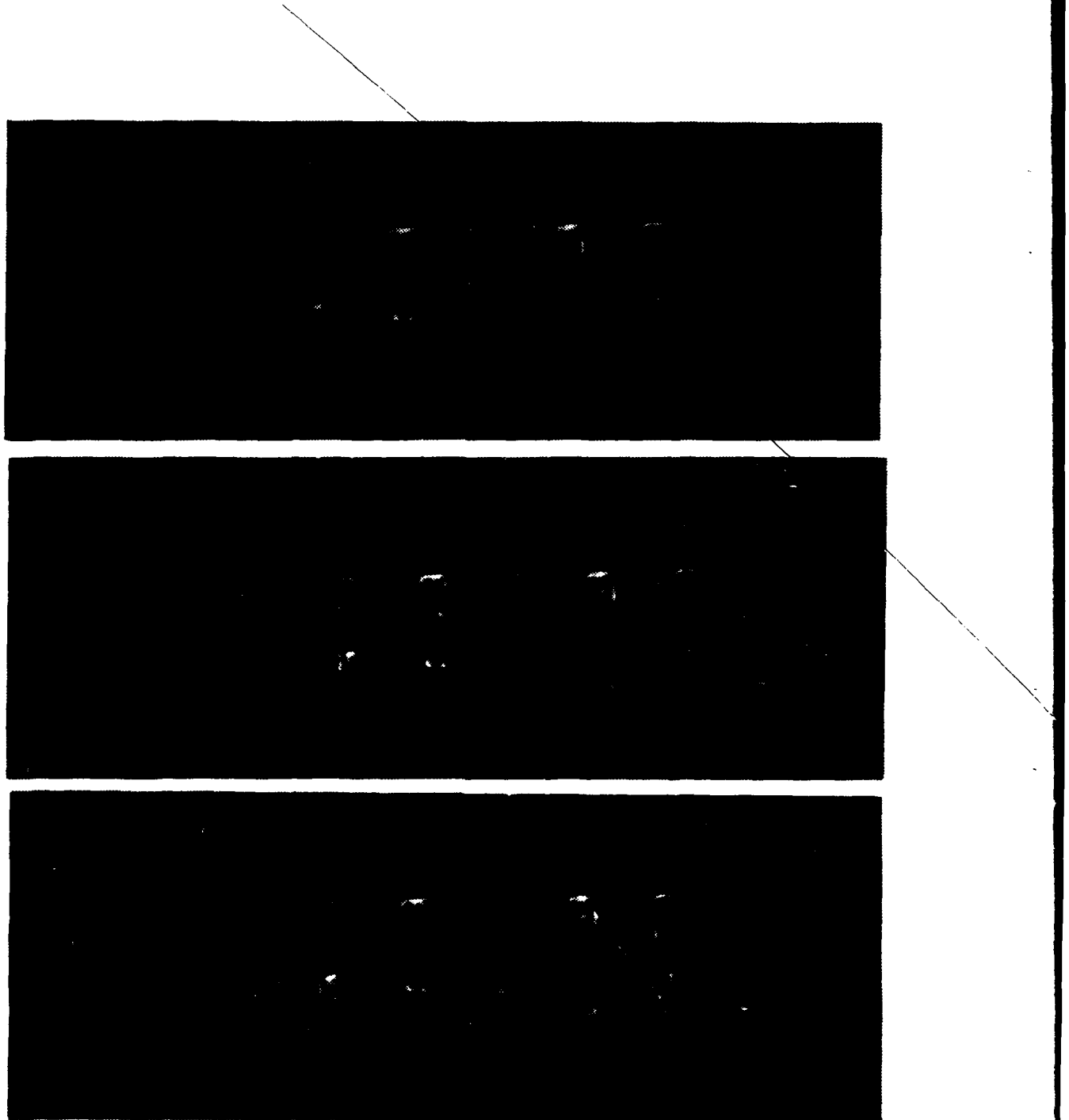


Figure 3.2: Flow in the x-z Plane at 0.2, 1.0 and 2.0 Watts

B. QUANTITATIVE

Figure 3.3 is a non-dimensional representation of local temperature excess levels measured at all thermocouple locations for an input power level of 2.0 watts. As expected, the measured component center temperatures were the highest. The top edge temperatures always exceeded the temperatures at the other edges. The left and right edge temperatures differed by a maximum of 22% at 2.0 watts. The heater strip had an 11 mm tab on the left side for power lead connections. Left edge conduction losses were therefore expected to be greater than the right side, resulting in slightly lower temperatures on the left. After the third component, the bottom edge temperatures exceeded the excess temperature of the sides. The side edges benefited more from fluid entrainment than the bottoms which are in the wake of the heated upstream components. In all experiments, the right edge temperature for component seven was lower than the established trend. It is believed that the thermocouple placement at this location may have slipped when the heater foil was pressed into place.

Heat transfer coefficients were computed from the data as outlined in equation 2.6. They indicated a downstream decreasing trend at a given power level. This is expected since the non-dimensional temperature excess is inversely proportional to h . As seen in Figure 3.3, the general trend tends to be increasing downstream excess temperatures.

As the component heat flux is increased, the buoyant flow becomes more vigorous. The component temperature levels, as a result, decrease. The calculated heat transfer coefficients are greater than those for the same component at lower power levels. With the larger values of h at higher power levels, there is a corresponding decrease in the non-dimensional temperature excess.

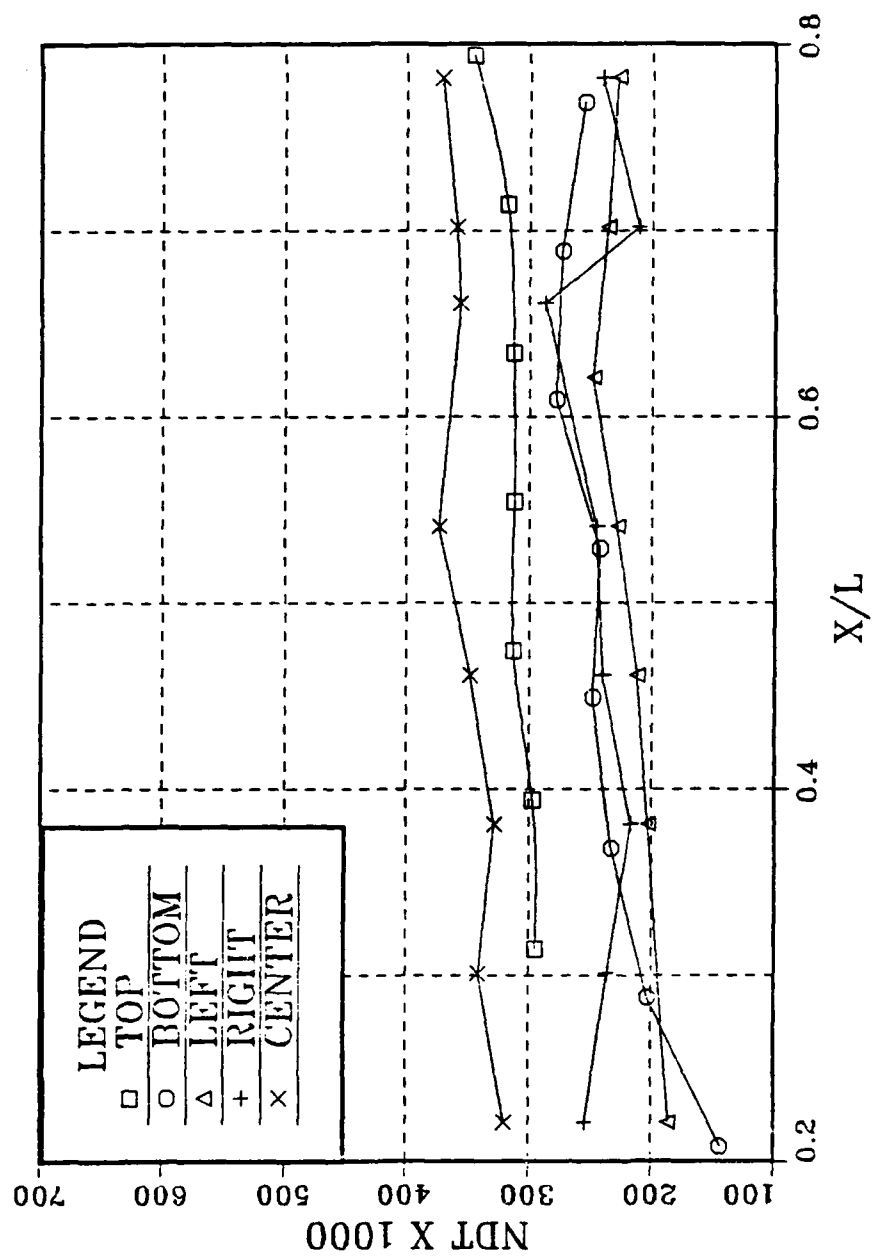


Figure 3.3: Non-dimensional Temperature Excess vs. Position: 2.0 Watts

Figure 3.4 is a logarithmic scatter plot of Nu vs. Gr^* . The cluster of data points at approximately a single Gr^* represents the Nusselt numbers for component centers at each power level. The Nusselt numbers decrease for downstream components, due to the increasing component temperatures.

As in the previous study, a modified Nusselt number, Nu^* , was calculated by using a scaling factor to account for the increase in convected energy of the flow at downstream locations.

$$Nu^* = Nu_n \times S_n^{\frac{1}{14}} \quad (3.1)$$

Nu_n and S_n are the local Nusselt numbers with the respective heater element numbers.

This modified data is plotted in Figure 3.5. The linear least squares fit through the data with a $\pm 5\%$ band is also presented. Using the scaling factor above, nearly all of the modified data falls within this band. Based on this curve fit, the following heat transfer relationship for the given array geometry was obtained:

$$Nu^* = 1.115(Gr^*)^{.12} \quad (3.2)$$

for $250 < Gr^* < 7000$ and $Pr \sim 7$.

C. EFFECT OF COMPONENT SPACING ON HEAT TRANSFER

Now that a heat transfer correlation has been developed for the given geometry of the array, it is desired to see how a change in component spacing would affect these relationships. This was achieved by powering every other and every third heater. This had the same effect as heater elements spaced 50.8 mm and 76.2 mm center to center. The resulting variations of non-dimensional temperature excess at the heater centers are shown in Figures 3.6 and 3.7.

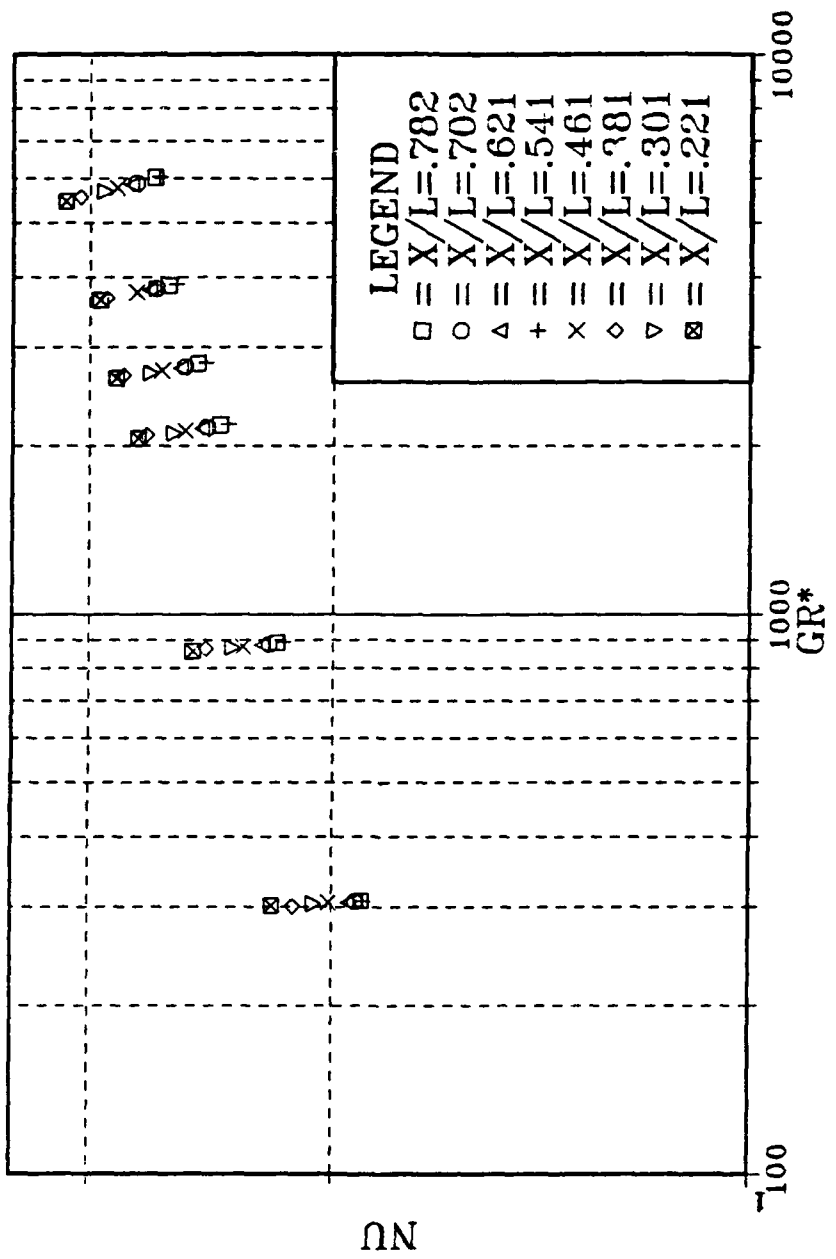


Figure 3.4: Data for Nusselt Number vs. Flux-Based Grashof Number

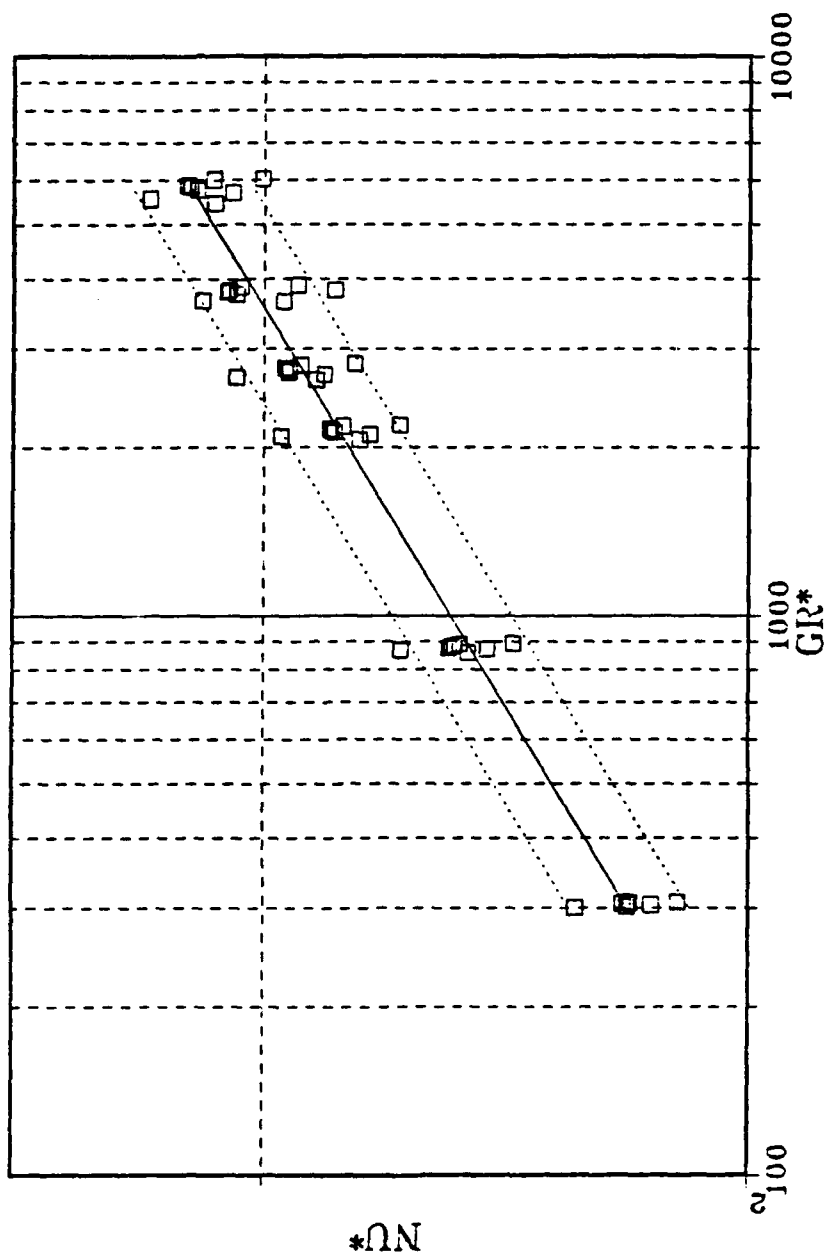


Figure 3.5: Modified Nusselt Number vs. Flux-Based Grashof Number with Least Squares Fit

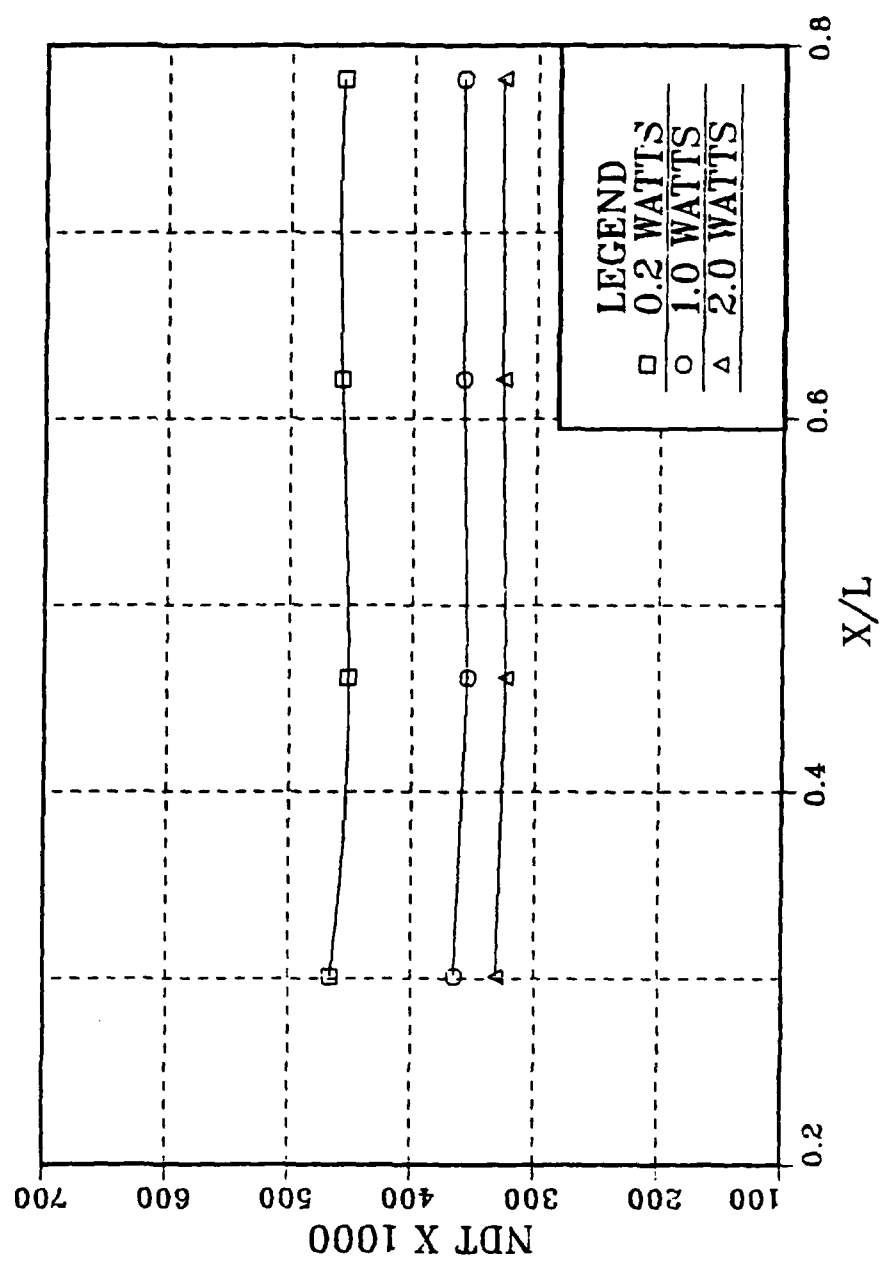


Figure 3.6: Non-dimensional Temperature Excess vs. Position with Four Elements Powered

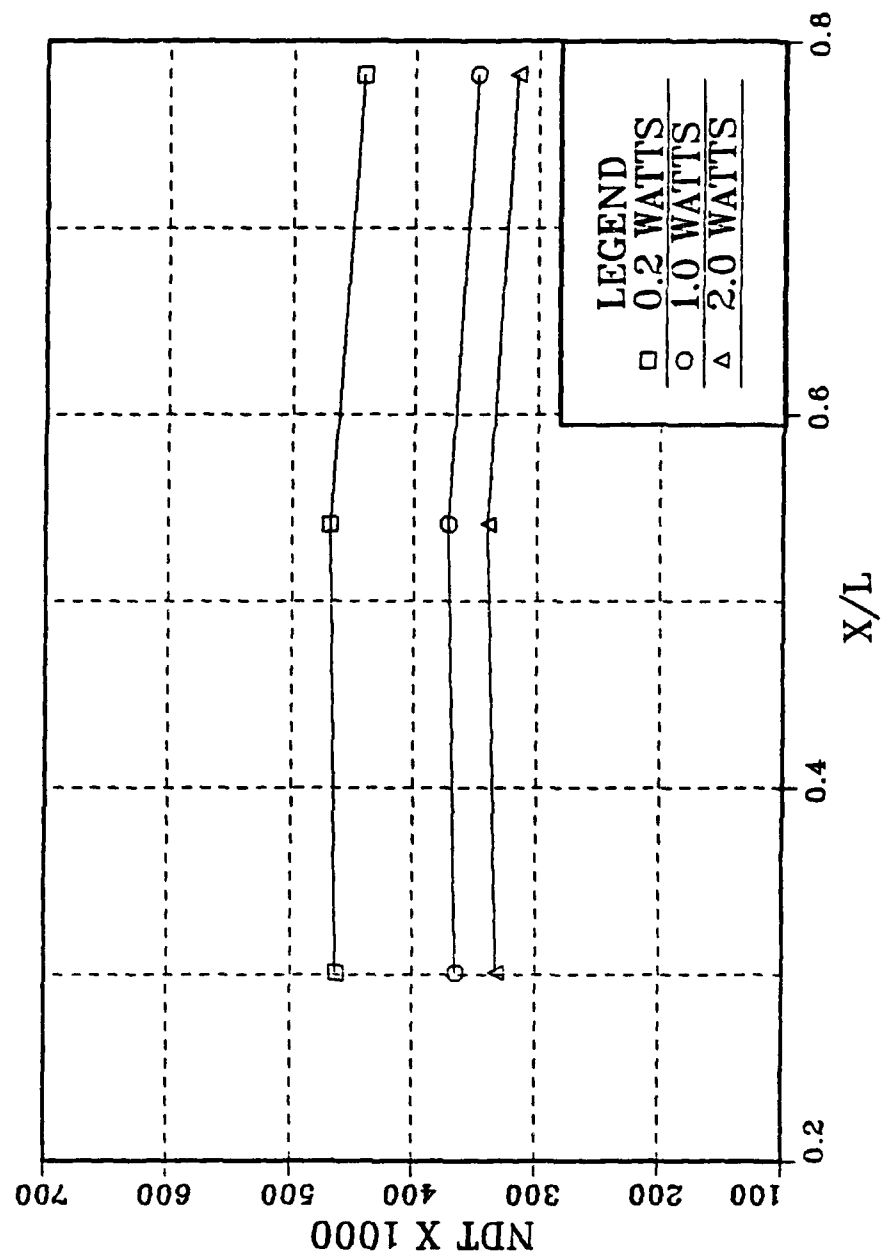


Figure 3.7: Non-dimensional Temperature Excess vs. Position with Three Elements Powered

When heaters 2, 4, 6 and 8 are powered, there is a slight decrease in the non-dimensional temperature at the first downstream component beyond the leading heater. Further up, component temperatures vary little from that of the second heater. When heaters 2, 5, and 8 are powered, the first two component temperatures remain unchanged. The trailing heater has a small drop in its non-dimensional temperature.

For the increased component spacings in Figures 3.6 and 3.7, the convected energy due to upstream heaters has only a weak effect on downstream components. The fluid momentum resulting from the buoyancy forces actually provides moderate improvement in heat transfer for the downstream heaters. Heat transfer relationships were obtained for all components by treating the elements in the array as single heaters. The resulting component based Nusselt numbers became almost independent of the downstream component position in the expanded array. These are plotted against the flux-based Grashof number in Figures 3.8 and 3.9. The least square fit to the correlated data for all unshrouded heaters is shown for comparison in each figure.

D. TEMPERATURE MEASUREMENTS WITHIN THE FLUID

Measurements of the thermal transport in the fluid adjacent to the test surface were made using the movable thermocouple probe. The thermocouple junction was initially centered on each component and then moved outward in the direction normal to the substrate. Temperatures are seen in Figure 3.10 for input power levels of 0.2 and 1.0 watts. The thermal boundary layer in both cases is well within the momentum exchange region which is approximately 1.6 cm thick for component 8 at 1.0 watt. This is expected due to the relatively large Pr of about 7.0 for water.

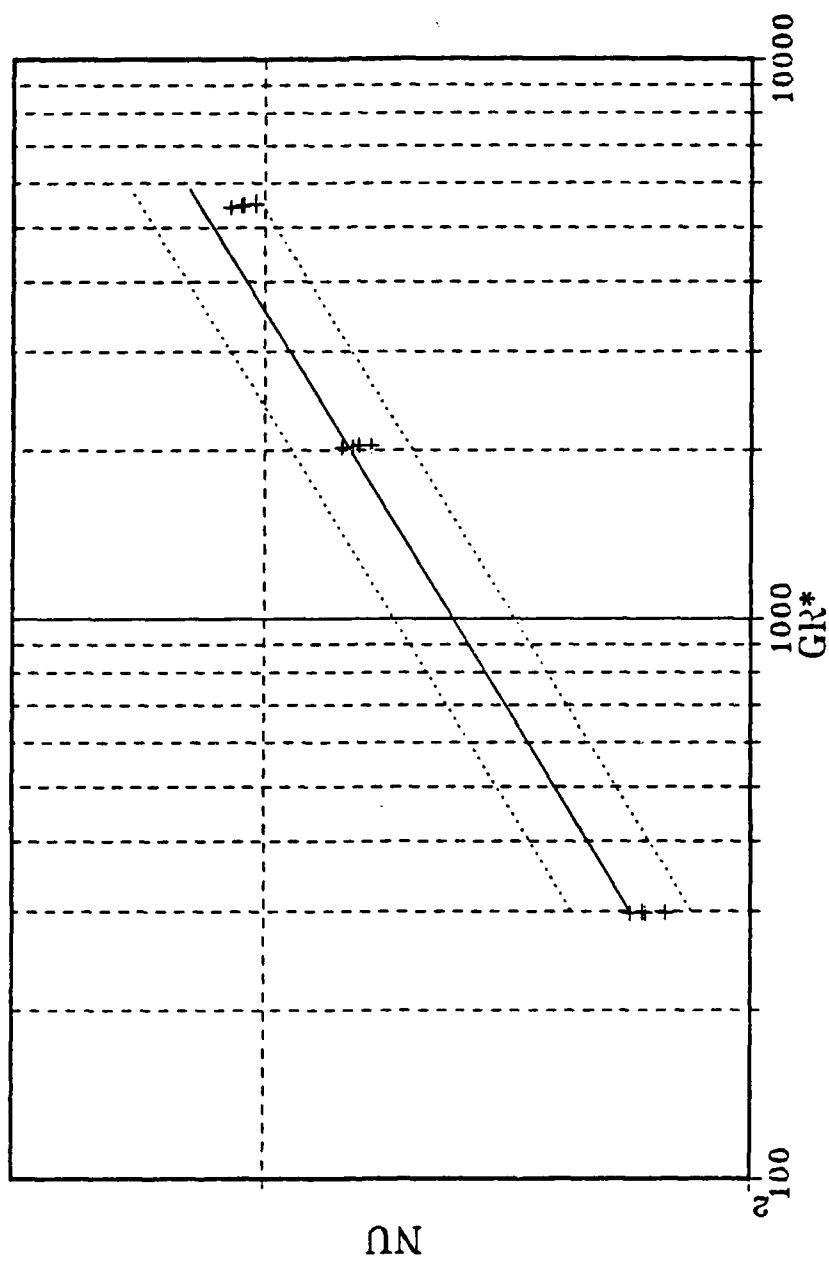


Figure 3.8: Nusselt Number vs. Flux-based Grashof Number with Four Elements Powered

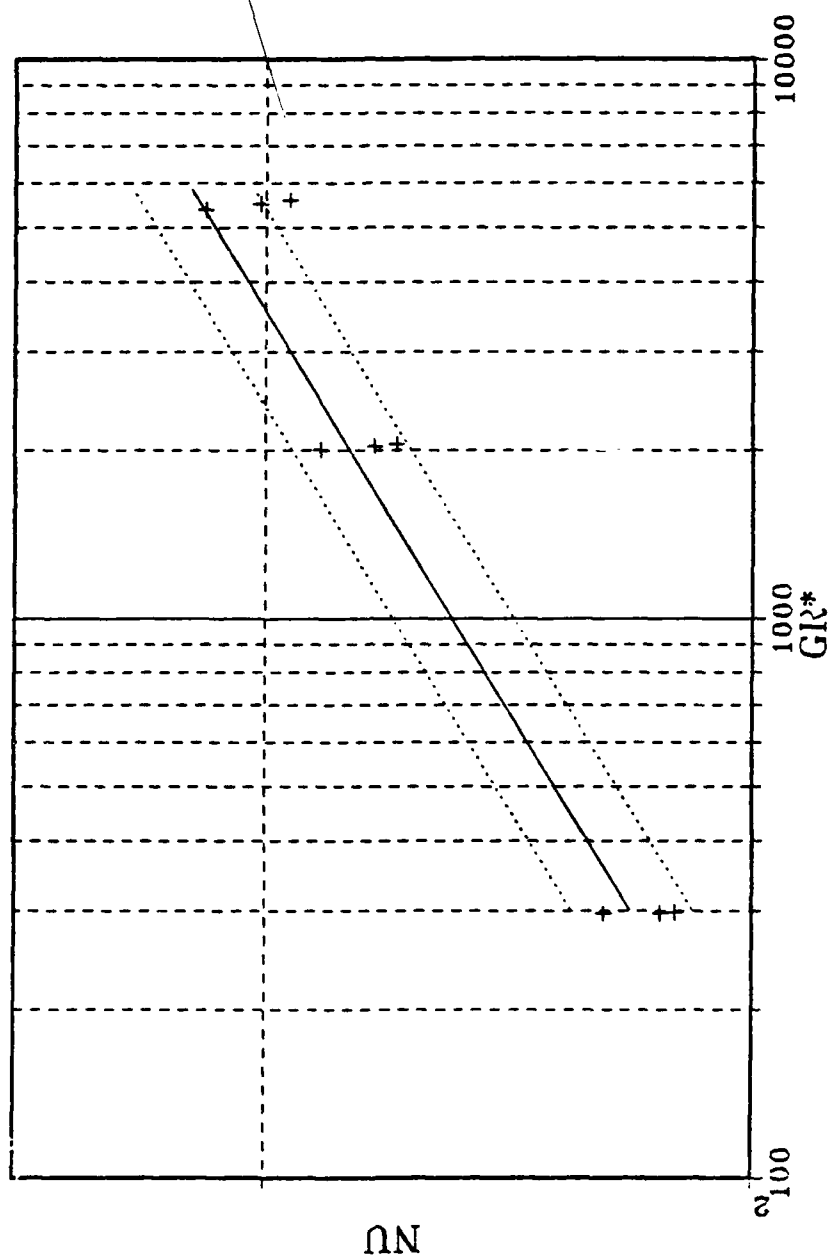


Figure 3.9: Nusselt Number vs. Flux-based Grashof Number with Three Elements Powered

Figure 3.10 suggests that it may be possible to move a shroud wall to within one component height without changing the rate of heat transfer significantly.

The traversing probe was slowly swept spanwise in the z-direction past the centers of the heaters 3, 5 and 8 at a distance of 1.0 mm outward in the y-direction from the heater surface. Resulting temperature variations are shown in Figure 3.11 for a power level of 1.0 watt. The component center is referred to as 0.0. A scale line provides a reference for the width of the heated region of each component. A large drop in temperature is seen to occur beyond $Z = \pm 6$ mm. For the center 50% of each heater, there is relatively small change in temperature, again suggesting a largely two dimensional flow there.

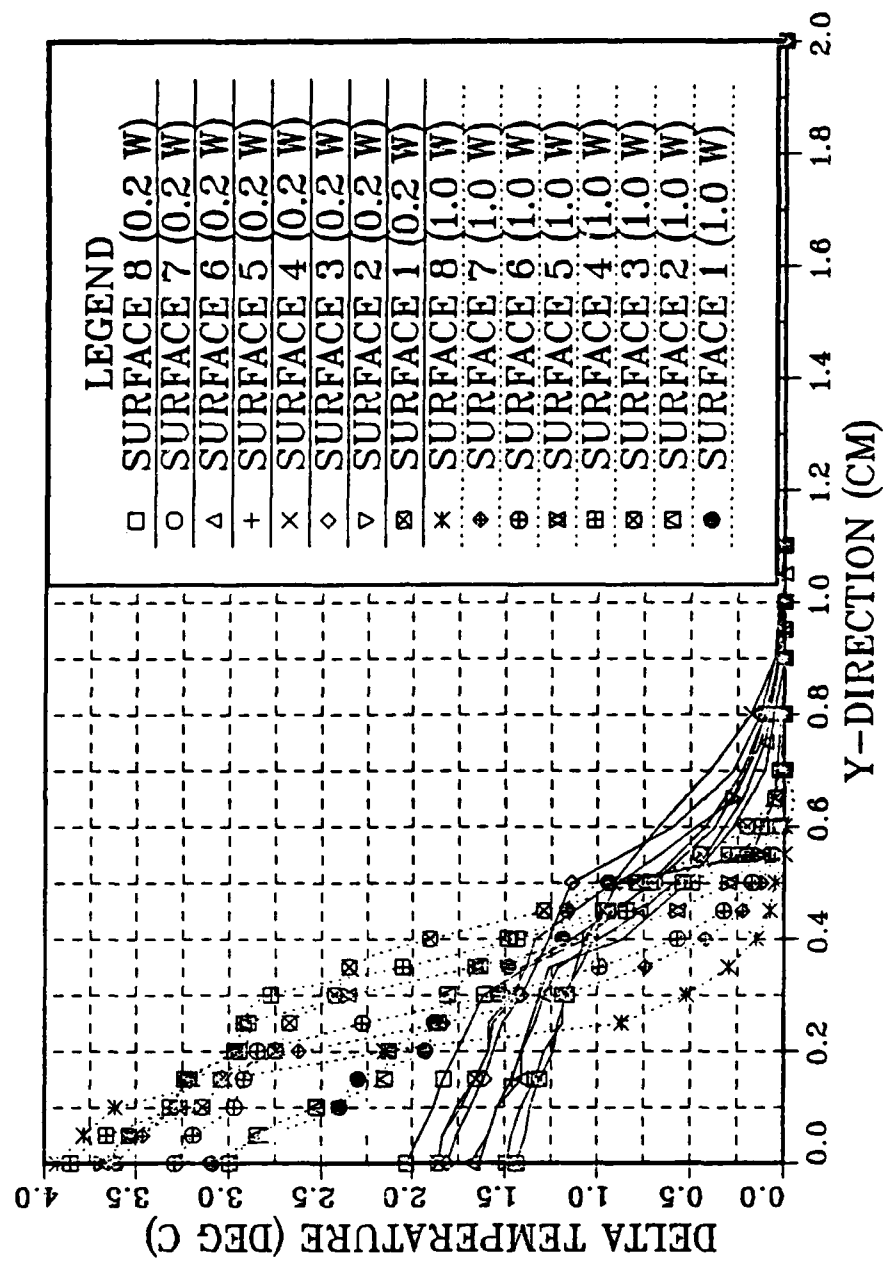


Figure 3.10: Fluid Temperature Distribution in the y-Direction for 0.2 and 1.0 Watts

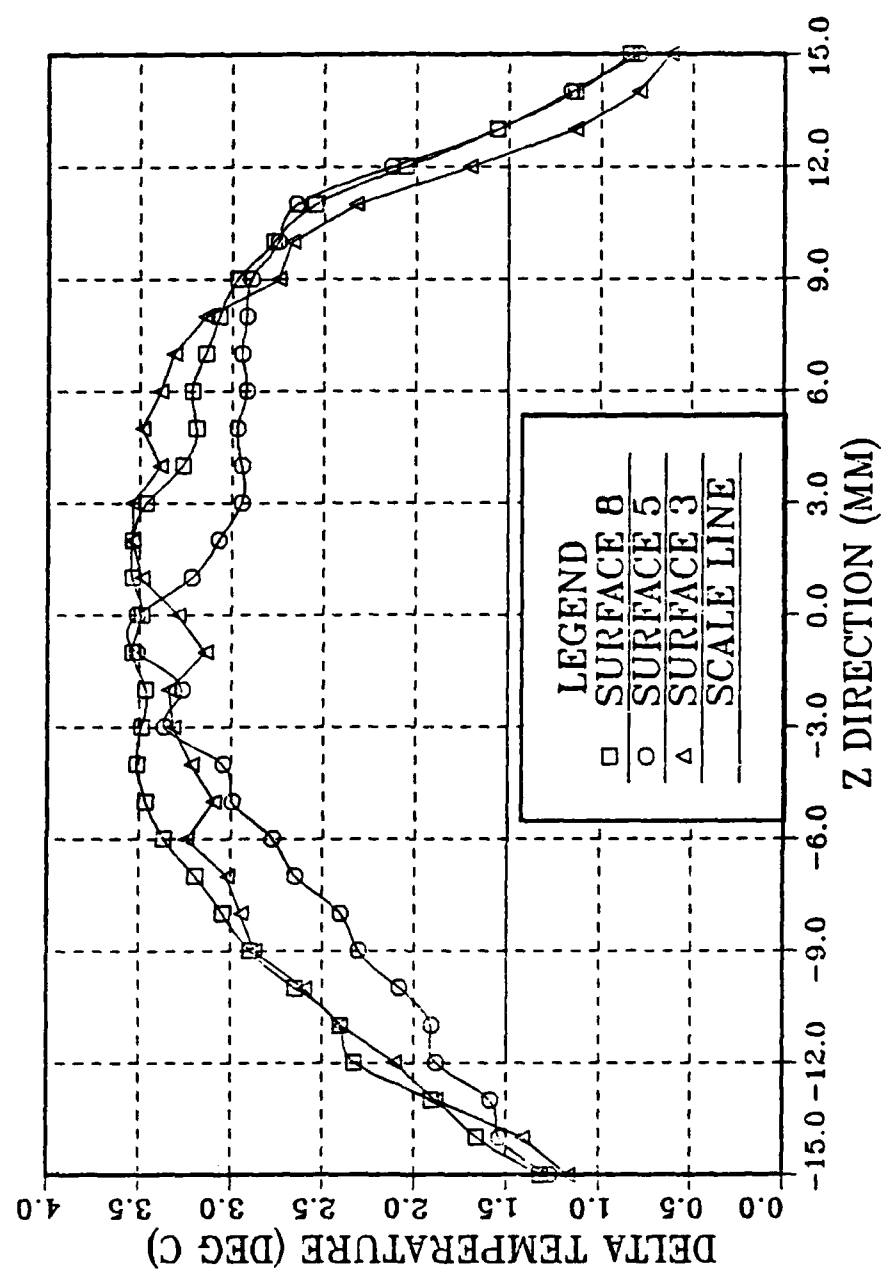


Figure 3.11: Spanwise Fluid Temperature Distribution

IV. TRANSPORT IN A VERTICAL CHANNEL

A plexiglass shroud, simulating the back side of a neighboring circuit board, was positioned to form a vertical channel of various widths.

A. FLOW VISUALIZATION

Useful photographs could only be taken with the shroud positioned no closer than 12 mm from the substrate. All visualizations presented are at power levels of 0.2, 1.0 and 2.0 watts respectively. Figure 4.1 shows the natural convection flow in the x-y plane with the shroud positioned 12 mm from the substrate. The shroud only allows entrainment from the sides and bottom. Initially the flow is not parallel to the channel walls. The entrained fluid entering from the bottom has velocity components in the x and y directions. As the boundary layer develops to the width of the channel, the flow is straightened and conforms to the channel. This same flow behavior occurs when the channel width is increased to 15 mm as shown in Figure 4.2. The effects of entrainment are more noticeable downstream since the boundary layer has more time to develop with the wider channel.

Figure 4.3 presents flow visualization in the x-y plane with the shroud positioned 6 mm from the substrate. These photographs were taken with the camera aligned in the direction normal to the surface. With the shroud in position, side entrainment is much more pronounced than the case without a shroud [Figure 3.2].

B. QUANTITATIVE

Figures 4.4 and 4.5 are non-dimensional representations of temperature excess levels for all center located thermocouples for each shroud condition. These two



Figure 4.1: Steady Flow in the x-y Plane for Power Levels of 0.2, 1.0 and 2.0 Watts with 12 mm Shroud

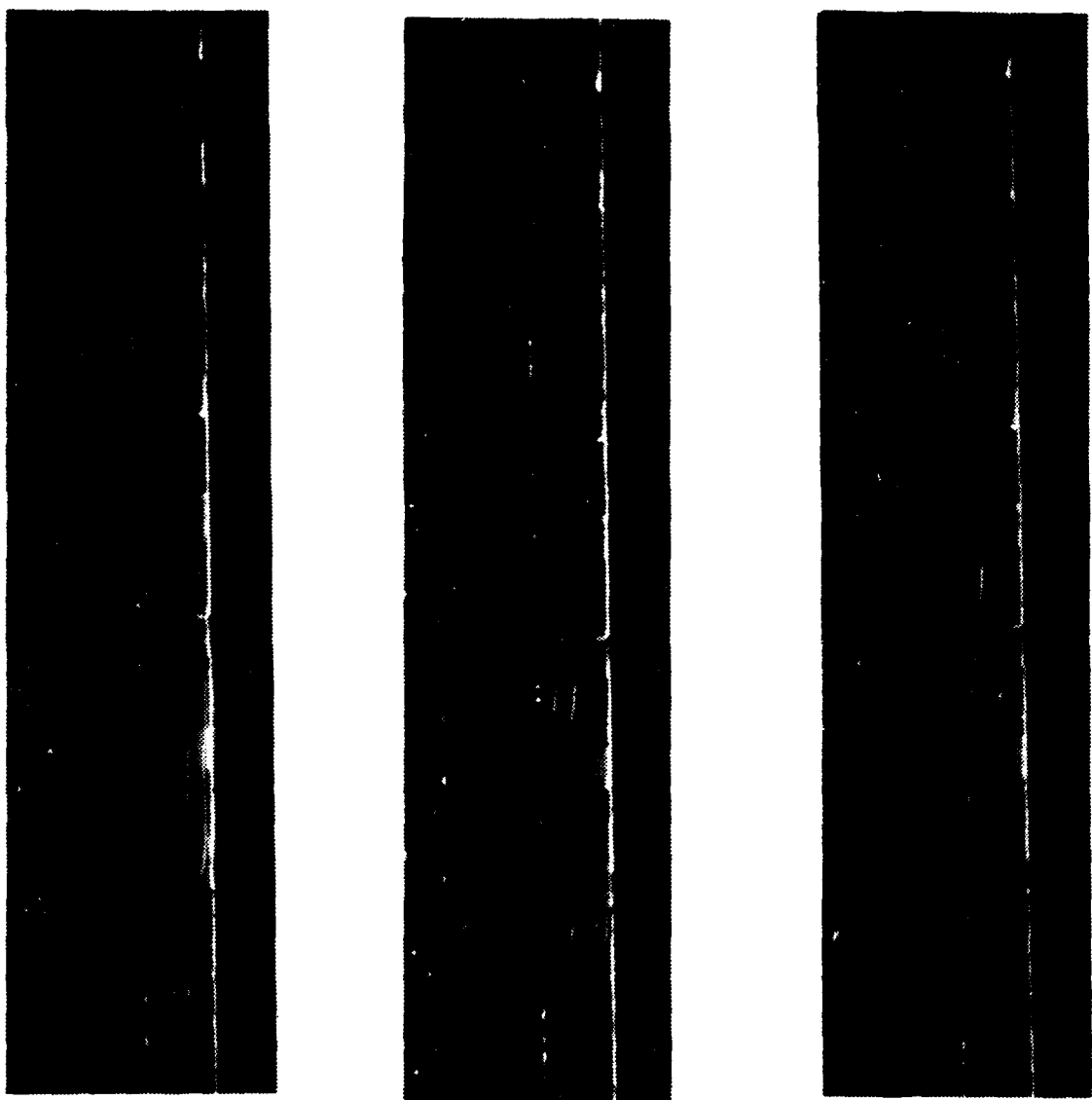


Figure 4.2: Steady Flow in the x-y Plane for Power Levels of 0.2, 1.0, 2.0 Watts with 15 mm Shroud

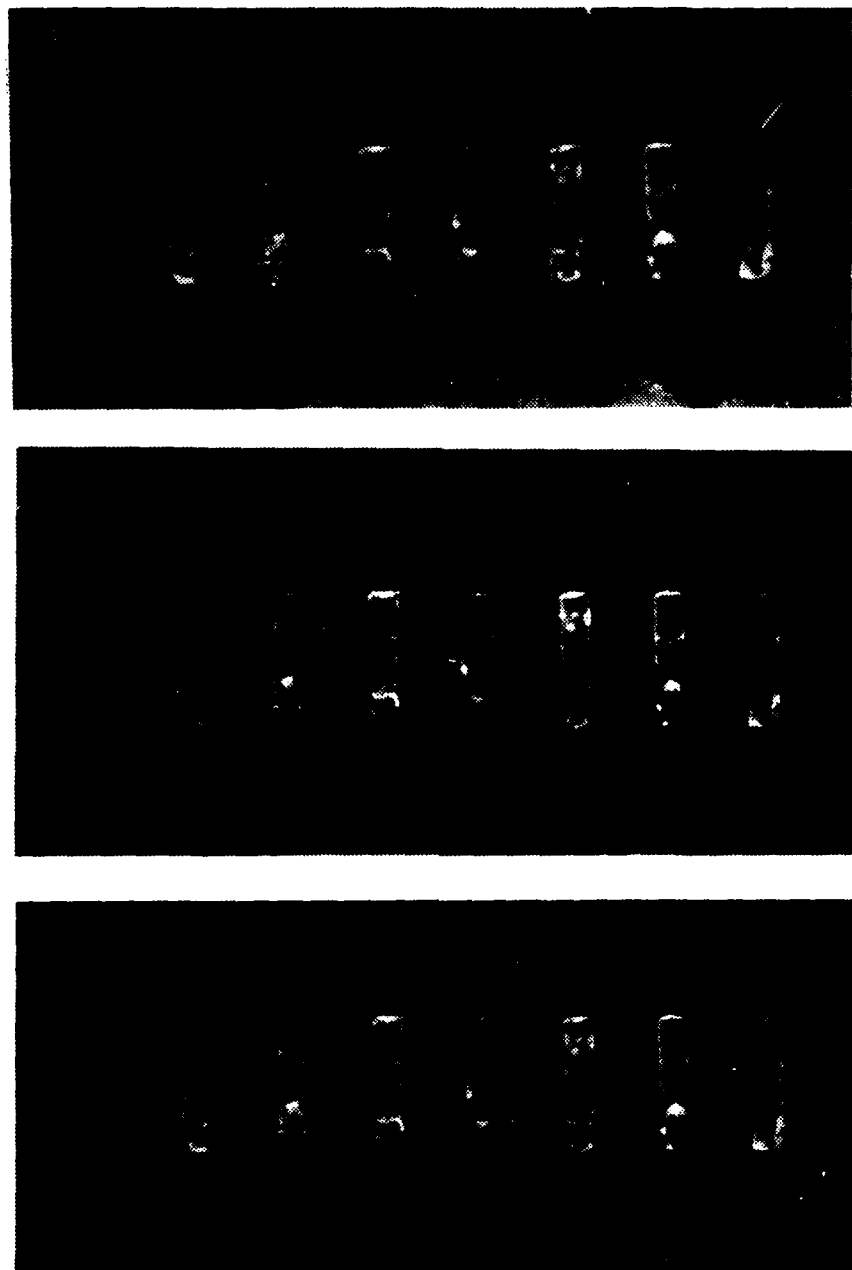


Figure 4.3: Flow in the x-z Plane with 6 mm Shroud Wall

figures depict the spread in data on the same plotting scale for the maximum and minimum power levels.

Again it is noted that the general trend, regardless of input power level, is increasing downstream temperature excess. As power is increased from 0.2 watts to 2.0 watts, the values for the non-dimensional temperature excess decrease. As expected, the heat transfer coefficient increases for corresponding components as the power level increases.

There is little difference in the non-dimensional temperature excess as the shroud is positioned 6 mm or more from the substrate. When the shroud is closer to the substrate, it reduces the ambient fluid entrainment, thereby increasing component temperatures. This is less pronounced at the higher power levels as seen in Figure 4.5.

Figure 4.6 shows the actual temperature difference for the component centers versus the shroud position at 2.0 watts. For this case and all other power levels, the actual temperature difference was greater when the shroud was closer than 6 mm from the substrate. When positioned 6 mm or more from the test surface, the actual temperature difference was within 0.5°C of the unshrouded levels.

The modified Nusselt numbers for component centers were calculated using the same correlation as in the previous chapter. These values were compared on a logarithmic plot with the flux-based Grashof numbers at each shroud position. The base line curve for the linear least squares fit of the unshrouded data with $\pm 5\%$ scatterband was also plotted for comparison. The scatter plot for data when the shroud was positioned 1.5 mm from the substrate is shown in Figure 4.7.

The only points in close agreement with base line data are those points corresponding to the leading heater element. Regardless of power level or shroud position, the leading heater can be treated as a single discrete heat source independent

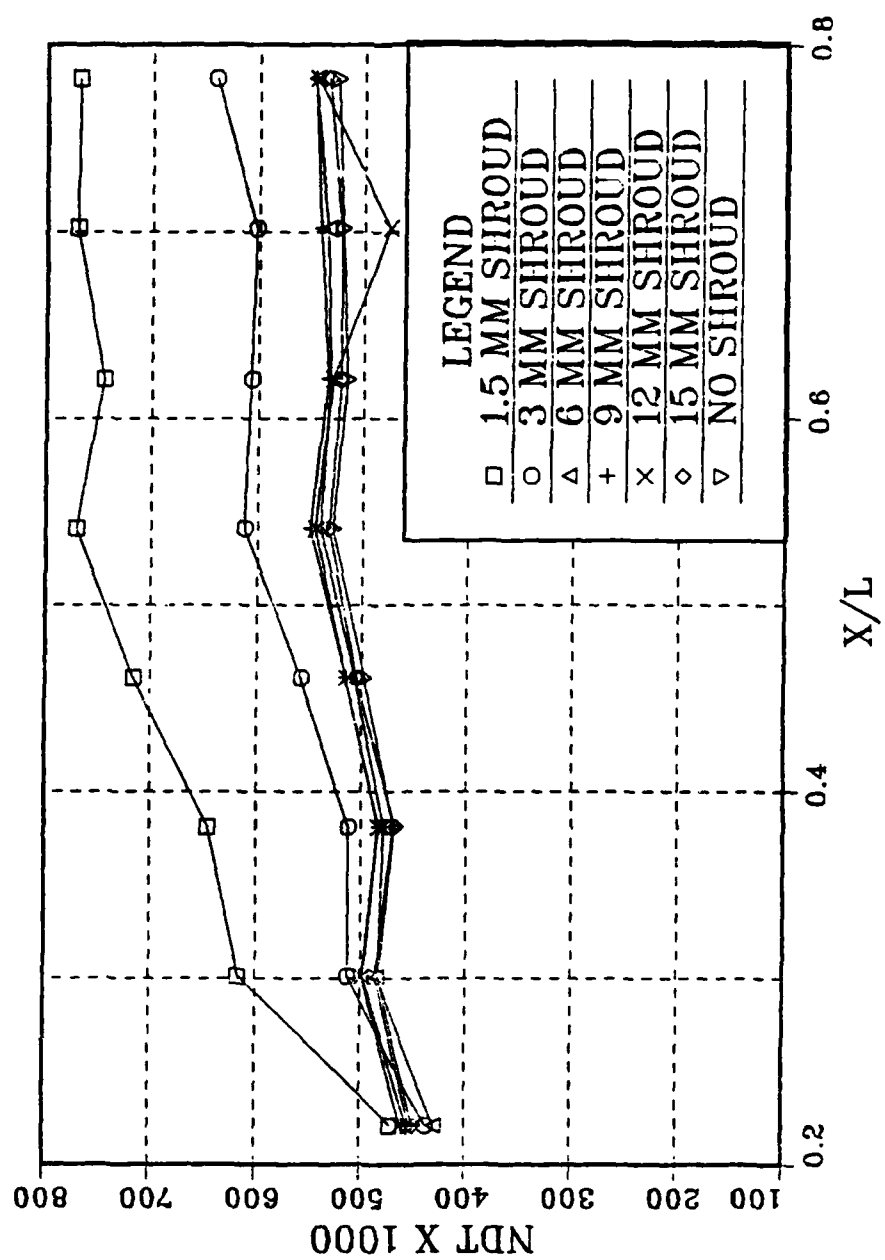


Figure 4.4: Non-dimensional Temperature Excess vs. Position with Shroud at 0.2 Watts

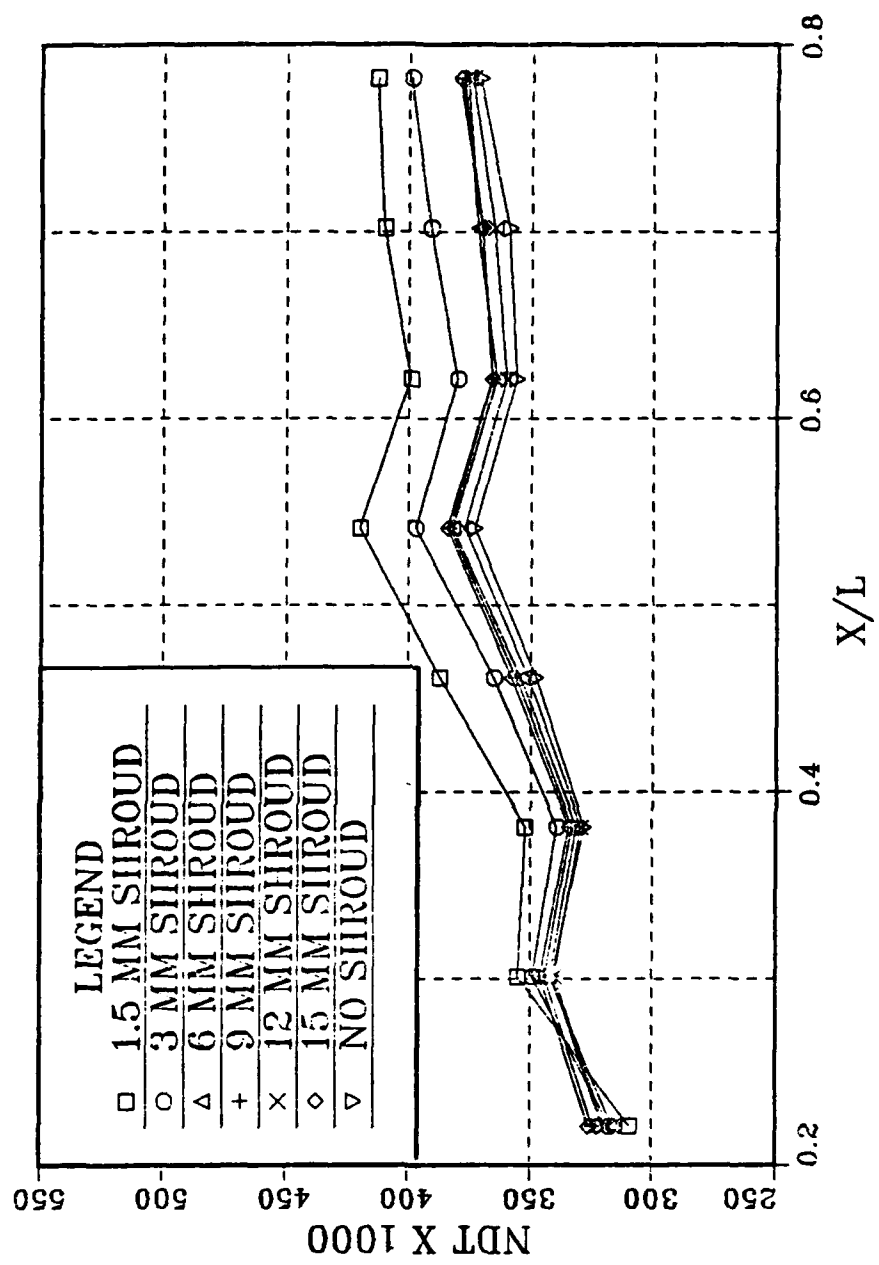


Figure 4.5: Non-dimensional Temperature Excess vs. Position with Shroud at 2.0 Watts

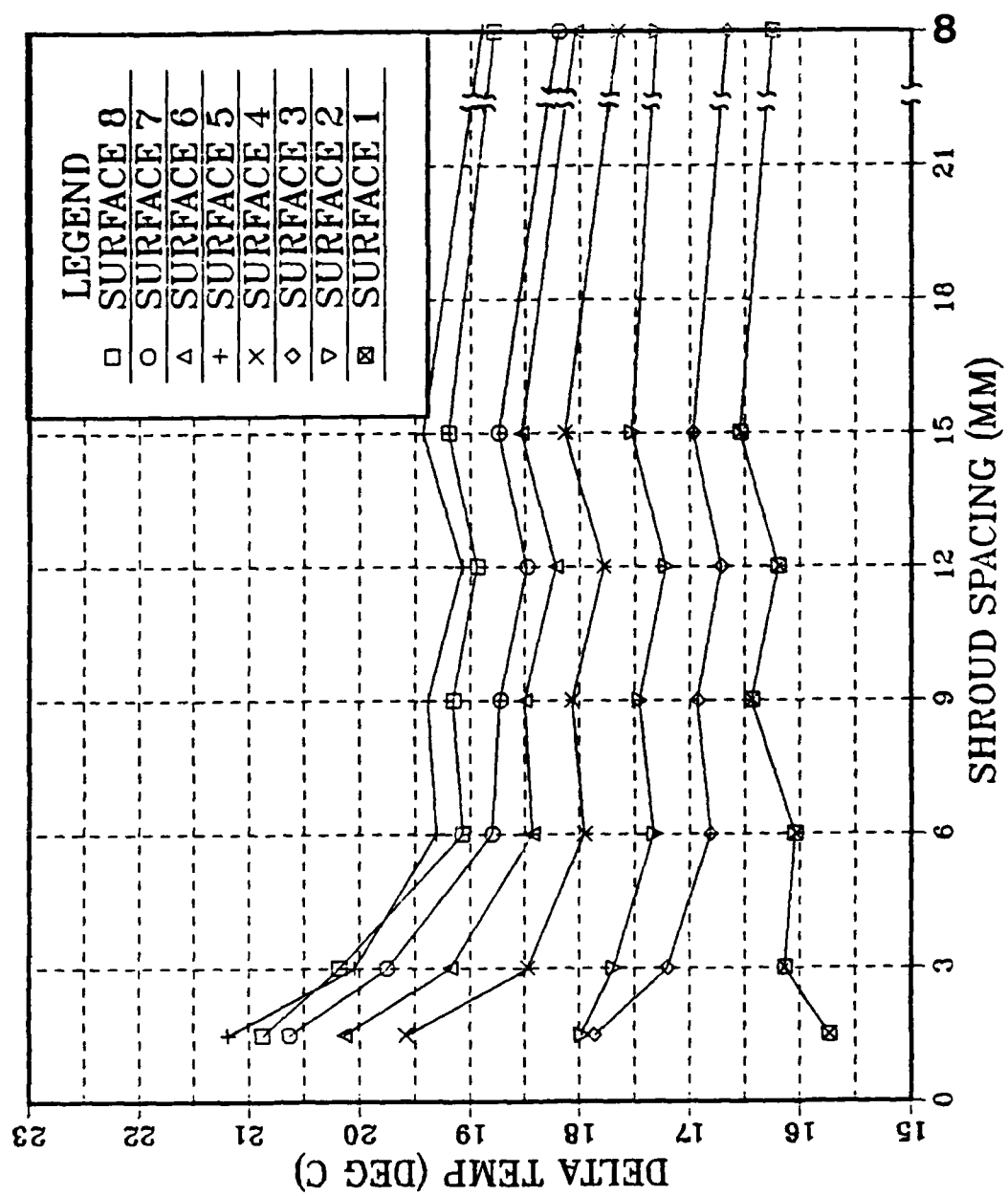


Figure 4.6: Temperature Difference vs. Shroud Spacing: 2.0 Watts

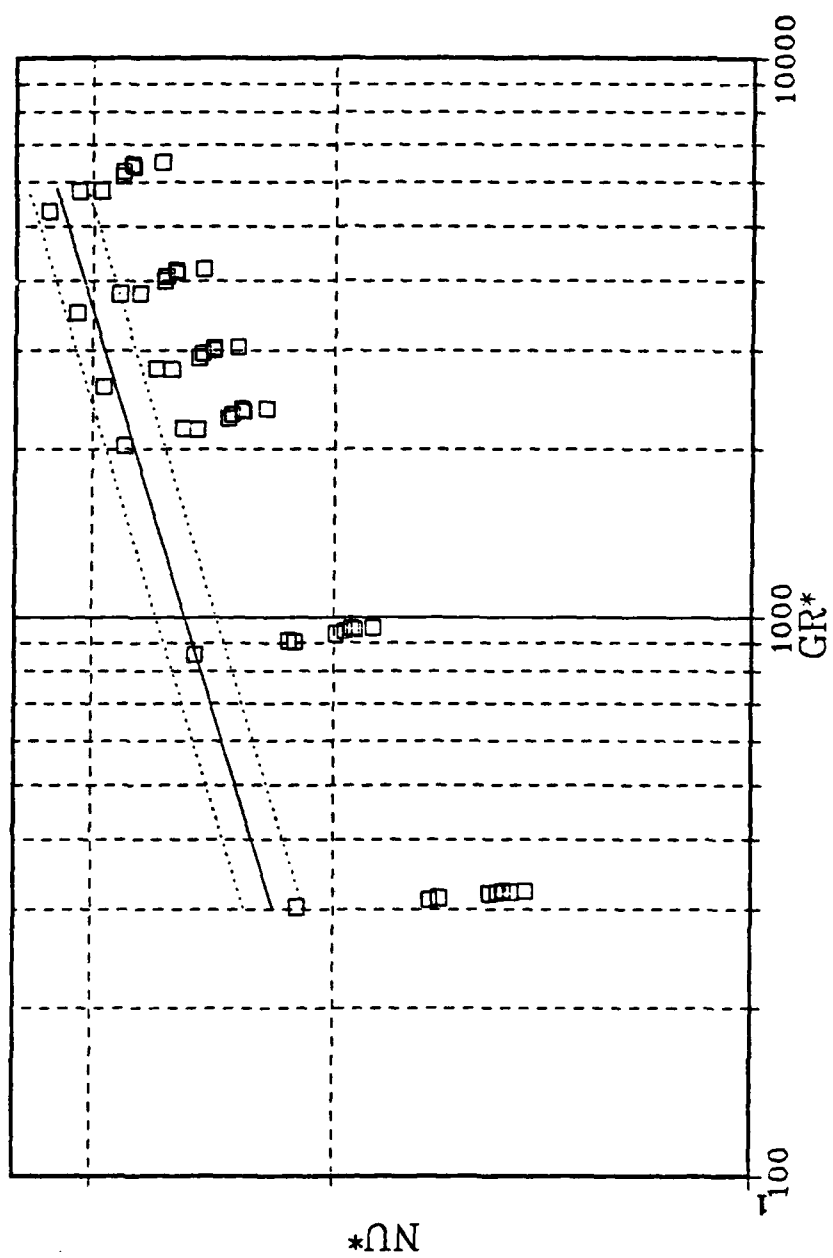


Figure 4.7: Modified Nusselt Number vs. Flux-based Grashof Number with Shroud at 1.5 mm

of downstream array geometry. A scatter plot of data for the shroud position of 3.0 mm is not much better than the previous case.

Figure 4.8 shows a plot of modified data when the shroud spacing is increased to 6.0 mm. The same trends seen here were found at all larger spacings. All data are seen to be in close agreement with the correlating equation thus, with a channel width of 6.0 mm or more in width and for the given geometric array, the modified Nusselt number can be calculated to within 5% accuracy using Equation 3.2 for $250 < Gr_x^* < 7000$ and $Pr \sim 7$.

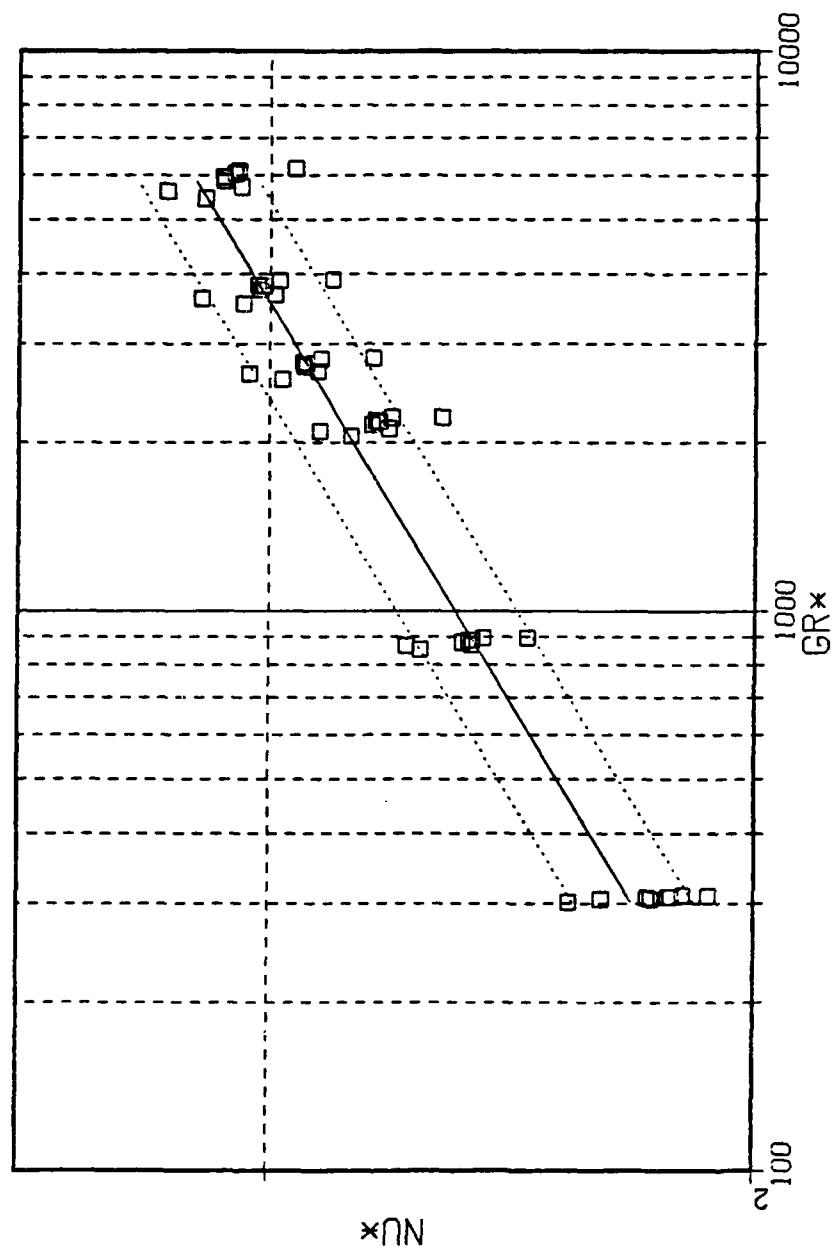


Figure 4.8: Modified Nusselt Number vs. Flux-based Grashof Number with Shroud at 6.0 mm

V. CONCLUSIONS

Flow visualization and quantitative analysis provided several significant conclusions:

- The flow was laminar over the given range of power levels.
- The convective flow is nearly two-dimensional when the shroud is not present. This condition greatly simplifies computational modelling of such flows.
- A thermal layer was embedded within the momentum region. This layer became thinner at increasing levels of heat flux.
- A general trend of increasing component temperatures downstream at each power level was found.
- No significant gain in the rate of heat transfer for channel widths of 6.0 mm or more was found over the unshrouded configuration.
- For geometrically similar arrays, heat transfer relationships for downstream components can be determined by using the correlating equation for this geometry.
- As component spacing is increased to two times or more of that for the present configuration, upstream effects become negligible and the heaters can be treated as an individual discrete heat source.

VI. RECOMMENDATIONS

In continuation of this study, it is suggested to use a similar array, however:

- Study the effects of even smaller component spacings on heat transfer.
- Flank each side of the single array with a column of flush mounted heat sources.
- Spray the heater elements with temperature sensitive liquid crystals.
- Measure the variation of temperature within the thermal layer at higher power levels for all components and spaces between components.
- Explore the transient evolution of transport.

APPENDIX A SOFTWARE

A. TEMPERATURE ACQUISITION PROGRAM

```

10
20      !!          TEMPERATURE ACQUISITION PROGRAM          !!
30      !!          (STEADY STATE)          !!
40
50      REAL Volts(60)
60      REAL Temp(59)
70      CREATE 8DAT " _____:700,0,_,";48
80      ASSIGN @Path3 TO " _____:700,0,_"
90      PRINT "                                     SURFACE #8"
100     PRINT
110     OUTPUT 709;"CONFMEAS DCV,100,USE 0"
120     ENTER 709:Volts(60)
130     OUTPUT 709;"CONFMEAS DCV,100-105,USE 0"
140     FOR I=0 TO 5
150     ENTER 709:Volts(I)
160     Temp(I)=.0006797+(25825.1328*Volts(I))-(607789.2467*(Volts(I)*Volts(I)))-(21952034.3364*(Volts(I)^3))+(8370810996.1874*(Volts(I)^4))+.075
170     PRINT "T. C.  #";I+1,"  Volts D.C.  ";Volts(I),"Temp. DEG. C ";Temp(I)
180     NEXT I
190     PRINT
200     PRINT "                                     SURFACE #7"
210     PRINT
220     OUTPUT 709;"CONFMEAS DCV,106-111,USE 0"
230     FOR I=6 TO 11
240     ENTER 709:Volts(I)
250     Temp(I)=.0006797+(25825.1328*Volts(I))-(607789.2467*(Volts(I)*Volts(I)))-(21952034.3364*(Volts(I)^3))+(8370810996.1874*(Volts(I)^4))+.075
260     PRINT "T. C.  #";I+1,"  Volts D.C.  ";Volts(I),"Temp. DEG. C ";Temp(I)
270     NEXT I
280     PRINT
290     PRINT "                                     SURFACE #6"
300     PRINT
310     OUTPUT 709;"CONFMEAS DCV,112-117,USE 0"
320     FOR I=12 TO 17
330     ENTER 709:Volts(I)
340     Temp(I)=.0006797+(25825.1328*Volts(I))-(607789.2467*(Volts(I)*Volts(I)))-(21952034.3364*(Volts(I)^3))+(8370810996.1874*(Volts(I)^4))+.075
350     PRINT "T. C.  #";I+1,"  Volts D.C.  ";Volts(I),"Temp. DEG. C ";Temp(I)
360     NEXT I

```

```

370 PRINT
380 PRINT " SURFACE #5
390 PRINT
400 OUTPUT 708; CONFMEAS DCV,118-119,USE 0"
410 FOR I=18 TO 19
420 ENTER 708:Volts(I)
430 Temp(I)=.0006797+(25825.1328*Volts(I))-(607769.2467*Volts(I)*Volts(I))-
21952034.3364*(Volts(I)^3)+(8370610996.1874*(Volts(I)^4))+.075
440 PRINT "T. C. #";I+1," Volts D.C. ";Volts(I),"Temp. DEG. C ";Temp(I)
450 NEXT I
460 OUTPUT 709;"CONFMEAS DCV,200-203,USE 0"
470 FOR I=20 TO 23
480 ENTER 709:Volts(I)
490 Temp(I)=.0006797+(25825.1328*Volts(I))-(607769.2467*Volts(I)*Volts(I))-
21952034.3364*(Volts(I)^3)+(8370610996.1874*(Volts(I)^4))+.075
500 PRINT "T. C. #";I+1," Volts D.C. ";Volts(I),"Temp. DEG. C ";Temp(I)
510 NEXT I
520 PRINT
530 PRINT " SURFACE #4"
540 PRINT
550 OUTPUT 708;"CONFMEAS DCV,204-208,USE 0"
560 FOR I=24 TO 29
570 ENTER 708:Volts(I)
580 Temp(I)=.0006797+(25825.1328*Volts(I))-(607769.2467*Volts(I)*Volts(I))-
21952034.3364*(Volts(I)^3)+(8370610996.1874*(Volts(I)^4))+.075
590 PRINT "T. C. #";I+1," Volts D.C. ";Volts(I),"Temp. DEG. C ";Temp(I)
600 NEXT I
610 PRINT
620 PRINT " SURFACE #3"
630 PRINT
640 OUTPUT 709;"CONFMEAS DCV,210-215,USE 0"
650 FOR I=30 TO 35
660 ENTER 709:Volts(I)
670 Temp(I)=.0006797+(25825.1328*Volts(I))-(607769.2467*Volts(I)*Volts(I))-
21952034.3364*(Volts(I)^3)+(8370610996.1874*(Volts(I)^4))+.075
680 PRINT "T. C. #";I+1," Volts D.C. ";Volts(I),"Temp. DEG. C ";Temp(I)
690 NEXT I
700 FOR J=1 TO 14
710 PRINT

```

```

720  NEXT J
730  PRINT " SURFACE #2"
740  PRINT
750  OUTPUT 709;"CONFMEAS DCV,216-219,USE 0"
760  FOR I=36 TO 39
770  ENTER 709;Volts(I)
780  Temp(I)=.0006797+(25825.1328*Volts(I))-(607789.2467*(Volts(I)*Volts(I))-
21952034.3364*(Volts(I)^3))+(8370810996.1874*(Volts(I)^4))+.075
790  PRINT "T. C. #";I+1," Volts D.C. ";Volts(I),"Temp. DEG. C ";Temp(I)
800  NEXT I
810  OUTPUT 709;"CONFMEAS DCV,300-301,USE 0"
820  FOR I=40 TO 41
830  ENTER 709;Volts(I)
840  Temp(I)=.0006797+(25825.1328*Volts(I))-(607789.2467*(Volts(I)*Volts(I)))-(21952034.3364*(Volts(I)^3))+(8370810996.1874*(Volts(I)^4))+.075
850  PRINT "T. C. #";I+1," Volts D.C. ";Volts(I),"Temp. DEG. C ";Temp(I)
860  NEXT I
870  PRINT
880  PRINT " SURFACE #1"
890  PRINT
900  OUTPUT 709;"CONFMEAS DCV,301-307,USE 0"
910  FOR I=42 TO 47
920  ENTER 709;Volts(I)
930  Temp(I)=.0006797+(25825.1328*Volts(I))-(607789.2467*(Volts(I)*Volts(I)))-(21952034.3364*(Volts(I)^3))+(8370810996.1874*(Volts(I)^4))+.075
940  PRINT "T. C. #";I+1," Volts D.C. ";Volts(I),"Temp. DEG. C ";Temp(I)
950  NEXT I
960  OUTPUT @Path3;Temp(+)
970  PRINT
980  PRINT
990  PRINT " BATH TEMPERATURES (TOP TO BOTTOM)"
1000  FFINT
1010  OUTPUT 709;"CONFMEAS DCV,317-319,USE 0"
1020  FOR I=57 TO 59
1030  ENTER 709;Volts(I)
1040  Temp(I)=.0006797+(25825.1328*Volts(I))-(607789.2467*(Volts(I)*Volts(I)))-(21952034.3364*(Volts(I)^3))+(6370810996.1874*(Volts(I)^4))+.075
1050  PRINT "VOLTS D.C. ";Volts(I),"TEMP. DEG. C ";Temp(I)
1060  NEXT I
1070  END

```

B. DATA REDUCTION PROGRAM

```
10 !-----  
20 !!-----  
30 !! DATA REDUCING PROGRAM  
40 !!-----  
50 !-----  
60 REAL T(48),Qcond(8)  
70 REAL Power,Tamb,G,Kpg,Delx,As,Per,Ta,Qconv,Lbar  
80 REAL Qflux,Deit,Tfilm,Beta,Svol,Dynvisc  
90 REAL Kinvisc,Kf,Pr,Theta,Ndt,Hx,Grmod,Hux,Lnu,Lgr  
100 PRINTER IS 1  
110 PRINT "INPUT DATA FILE NAME"  
120 INPUT Filenames$  
130 PRINT  
140 PRINT "INPUT POWER VALUE IN WATTS"  
150 INPUT Power  
160 PRINT  
170 PRINT "INPUT SHROUD SPACING IN mm"  
180 INPUT Space$  
190 PRINT  
200 PRINT "INPUT AMBIENT TEMPERATURE"  
210 INPUT Tamb  
220 PRINTER IS 701  
230 PRINT "POWER LEVEL (WATTS) : ",Power  
240 PRINT  
250 PRINT "SHROUD POSITION (mm) : ",Space$  
260 PRINT  
270 PRINT "AMBIENT TEMPERATURE (C) : ",Tamb  
280 PRINT  
290 PRINT  
300 ASSIGN @Path TO Filenames$  
310 ENTER @Path;T(*)  
320 G=9.81  
330 Kpg=.1421  
340 Delx=.006731  
350 As=.0239+.0078  
360 Per=2*.0239+2*.0078  
370 Lbar=As/Per  
380 A$="Qcond"
```

```

390  BS="X\1L"
400  CS="NET"
410  DS="LOG(Nux.)"
420  ES="LOG(Grx*)"
430  FS="DELT"
440  GS="Hx"
450  HS="Nux"
460  IS="Grx*"
470  !!!!!!! !!!!!!! !!!!!!! !!!!!!! !!!!!!! !!!!!!! !!!!!!!
480  ! COMPUTE CONDUCTION LOSSES !
490  !!!!!!! !!!!!!! !!!!!!! !!!!!!! !!!!!!! !!!!!!! !!!!!!!
500  J=8
510  FOR I=0 TO 42 STEP 6
520  Ta=(T(I)+T(I+1)+T(I+2)+T(I+3)+T(I+4))/5
530  Qcond(J)=As*Kpg*(Ta-T(I+5))/Delx
540  J=J-1
550  NEXT I
560  !!!!!!! !!!!!!! !!!!!!! !!!!!!! !!!!!!! !!!!!!! !!!!!!!
570  N=0
580  FOR J=8 TO 1 STEP -1
590  Cnt=0
600  Xf=((J-1)*25.4+74)/317
610  Xb=((J-1)*25.4+66)/317
620  Xc=((J-1)*25.4+70)/317
630  PRINT
640  PRINT
650  PRINT " SURFACE #",J
660  PRINT
670  PRINT USING "2X,AAAAA,4X,AAA,4X,AA,4X,AAAAAAAAA,2X,AAAAAAAAAA,3X,AAAA,5X,AA
,5X,AA,4X,AAA";A$,B$,C$,D$,E$,F$,G$,H$,I$
680  FOR I=N TO N+4
690  Qconv=Power-Qcond(J)
700  Qflu=Qconv/As
710  Delt=T(I)-Tamb
720  Tfilm=273.15+(T(I)+Tamb)/2
730  Beta=(-7.944856E-8*(Tfilm^2))+(5.7356479E-5*Tfilm)-.0097810563
740  Spvol=(4.69699E-9*(Tfilm^2))+(-2.53745E-6*Tfilm)+.001341903
750  Dynvisc=(3.2348511E-7*(Tfilm^2))+(-.00021474487*Tfilm)+.036166792
760  Kinvisc=Spvol*Dynvisc

```

```

770 Kf=(1.418181818E-3*Tfilm)+.1866
780 Pr=(4.65706E-3*(Tfilm^2))+(-0.922094*Tfilm)+463.3319
790 Theta=Qflux*Lbar/Kf
800 Ndt=Delt/Theta
810 Hx=Qflux/Delt
820 Grmod=(G*Beta*Qflux*(Lbar)^4)/(Kf*Kinvisc^2)
830 Nux=Hx*Lbar/Kf
840 Lgr=LGT(Grmod)
850 Lnu=LGT(Nux)
860 IF Cnt=0 THEN Xtol=Xt
870 IF Cnt=1 THEN Xtol=Xb
880 IF Cnt>1 THEN Xtol=Xc
890 Cnt=Cnt+1
900 PRINT USING "1X,0.0000,2X,0.000,2X,0.000,4X,0.000,7X,0.000,4X,00.000,2X,00
00.0,2X,00.000,2X,0000.0";Qcend(J),Xtol,Ndt,Lnu,Lgr,Delt,Hx,Nux,Grmod
910 NEXT I
920 N=N+2
930 NEXT J
940 END

```

APPENDIX B EQUATIONS

A. SAMPLE CALCULATIONS

These calculations are based on temperatures from data corresponding to surface eight with all elements powered to 1.0 Watt and no shroud.

1. CHARACTERISTIC DIMENSIONS

$$\begin{aligned} P &= 2(0.0078 + 0.0239) \\ &= 0.063m \end{aligned} \tag{B.1}$$

$$\begin{aligned} A_s &= (0.0078)(0.0239) \\ &= 1.864 \times 10^{-4} m^2 \end{aligned} \tag{B.2}$$

$$\begin{aligned} \bar{L} &= \frac{1.864 \times 10^{-4}}{0.0634} \\ &= 2.940 \times 10^{-3}m \end{aligned} \tag{B.3}$$

2. CONDUCTION LOSS

$$\begin{aligned} T_{avg} &= \frac{30.40 + 27.98 + 27.09 + 27.39 + 31.11}{5} \\ &= 28.79^\circ C \end{aligned} \tag{B.4}$$

$$\begin{aligned} Q_{COND} &= \frac{(1.864 \times 10^{-4})(0.1421)(28.79 - 26.09)}{.006731} \\ &= 0.0106W \end{aligned} \tag{B.5}$$

3. CONVECTED HEAT FLUX

$$Q_{CONV} = 1.0 - 0.0106$$

$$= 0.9894W \quad (B.6)$$

$$\begin{aligned} q'' &= \frac{0.9894}{1.864 \times 10^{-4}} \\ &= 5308 \frac{W}{m^2} \end{aligned} \quad (B.7)$$

4. FLUID PROPERTIES

$$\begin{aligned} T_{film} &= \frac{31.11 + 20.55}{2} + 273.15 \\ &= 298.98K \end{aligned} \quad (B.8)$$

$$\begin{aligned} \beta &= (-7.945 \times 10^{-8})(298.98) + (5.736 \times 10^{-5}) \\ &\quad (298.98) - 9.781 \times 10^{-3} \\ &= 2.665 \times 10^{-4} K^{-1} \end{aligned} \quad (B.9)$$

$$\begin{aligned} v &= (4.697 \times 10^{-9})(298.98)^2 - (2.537 \times 10^{-6})(298.98) \\ &\quad + 1.342 \times 10^{-3} \\ &= 1.003 \times 10^{-3} \frac{m^3}{kg} \end{aligned} \quad (B.10)$$

$$\begin{aligned} \mu &= (3.235 \times 10^{-7})(298.98)^2 - (2.147 \times 10^{-4})(298.98) \\ &\quad + 0.0362 \\ &= 9.264 \times 10^{-4} \frac{Ns}{m^2} \end{aligned} \quad (B.11)$$

$$\begin{aligned} \nu &= (1.003 \times 10^{-3})(9.264 \times 10^{-4}) \\ &= 9.262 \times 10^{-7} \frac{m^2}{s} \end{aligned} \quad (B.12)$$

$$\begin{aligned} k_f &= (1.418 \times 10^{-3})(298.98) + 0.1866 \\ &= 0.611 \frac{W}{mK} \end{aligned} \quad (B.13)$$

5. NON-DIMENSIONAL TEMPERATURE EXCESS

$$\theta = 31.11 - 20.55 = 10.56^\circ C \quad (B.14)$$

$$\theta_o = \frac{(5308)(2.940 \times 10^{-3})}{0.611} = 25.54^\circ C \quad (B.15)$$

$$NDT = \frac{10.56}{25.54} = 0.413 \quad (B.16)$$

6. HEAT TRANSFER COEFFICIENT

$$h_x = \frac{5308}{31.11 - 20.55} = 502.7 \frac{W}{m^2 K} \quad (B.17)$$

7. FLUX-BASED GRASHOF NUMBER

$$Gr_x^* = \frac{(9.81)(2.665 \times 10^{-4})(5308)(2.940 \times 10^{-3})^4}{(0.611)(9.292 \times 10^{-7})^2} = 1965 \quad (B.18)$$

8. NUSSELT NUMBER

$$Nu = \frac{(502.7)(2.940 \times 10^{-3})}{0.611} = 2.419 \quad (B.19)$$

LIST OF REFERENCES

1. Hannemann, R., Incropera, F. P., and Simons, R., "Single Phase Liquid Cooling," *Research Needs in Electronic Cooling*, pp. 6-25, December 1986.
2. Milanez, L. F. and Bergles, A. E., "Studies on Natural Convection Heat Transfer from Thermal Sources on a Vertical Surface," *Proceedings of the Eighth International Heat Transfer Conference*, Vol. 3, pp. 1347-1352, 1986.
3. Johnson, C. B., "Evaluation of Correlations for Natural Convection Cooling of Electronic Equipment," *Heat Transfer Engineering*, Vol. 7, pp. 36-45, 1986.
4. Park, K. A. and Bergles, A. E., "Natural Convection Heat Transfer Characteristics of Simulated Microelectronic Chips," *Journal of Heat Transfer - 1987, ASME, HTD-Vol. 109*, pp.90-96.
5. Hazard, S. J., "Single Phase Liquid Immersion Cooling of Discrete Heat Sources in a Vertical Channel," M.S.M.E. Thesis, Naval Postgraduate School, Monterey, CA , December 1987.
6. Baker, E., "Liquid Cooling of Microelectronic Devices by Free and Forced Convection," *Microelectronics and Reliability*, Pergamon Press, Vol. 11, pp. 213-222, 1972.
7. Willson, T. D., "A Study of Natural Convection Cooling of Multiple Discrete Heat Sources in a Vertical Channel," M.S.M.E. Thesis, Naval Postgraduate School, Monterey, CA , June 1988.
8. Incropera, F. P., and DeWitt, D. P., *Fundamentals of Heat and Mass Transfer*, p. 774, John Wiley and Sons, 1981.

INITIAL DISTRIBUTION LIST

	No. of Copies
1. Defense Technical Information Center Cameron Station Alexandria, VA 22304-6145	2
2. Library, Code 0142 Naval Postgraduate School Monterey, CA 93943-5002	2
3. Mr. Howard Stevens Head, Electrical Research Center David Taylor Research Center Annapolis, MD 21402	1
4. Superintendent Naval Postgraduate School Attn: Professor A. J. Healey, Code 69Hy Department of Mechanical Engineering Monterey, CA 93943-5004	1
5. Superintendent Naval Postgraduate School Attn: Professor Y. Joshi, Code 69Ji Department of Mechanical Engineering Monterey, CA 93943-5004	3
6. Superintendent Naval Postgraduate School Attn: Professor M. D. Kelleher, Code 69Kk Department of Mechanical Engineering Monterey, CA 93943-5004	1
7. Superintendent Naval Postgraduate School Attn: Professor A. D. Kraus, Code 62Ks Department of Electrical and Computer Engineering Monterey, CA 93943-5004	1

8. Mr. Duane Embree Naval Weapons Support Center Code 0642 Crane, IN 47522	1
9. Superintendent Naval Postgraduate School Attn: Curricular Officer, Code 34 Monterey, CA 93943-5004	1
10. Superintendent Naval Postgraduate School Attn: Lt. Al Gaiser SMC 2007 Monterey, CA 93943-5000	1
11. Mr. Joseph Cipriano Executive Director Weapons and Combat Systems Directorate Naval Sea Systems Command Washington, D.C. 20362-5101	1
12. Lt. Daniel L. Knight Rt. 1, Box 224A Warrenville, S.C. 29851	1